



HAL
open science

Boundary conditions at fluid porous interfaces

Christian Ruyer-Quil, Sanghasri Mukhopadhyay, R Usha

► **To cite this version:**

Christian Ruyer-Quil, Sanghasri Mukhopadhyay, R Usha. Boundary conditions at fluid porous interfaces. 2023. hal-04179827v1

HAL Id: hal-04179827

<https://hal.science/hal-04179827v1>

Preprint submitted on 10 Aug 2023 (v1), last revised 6 Sep 2024 (v2)

HAL is a multi-disciplinary open access archive for the deposit and dissemination of scientific research documents, whether they are published or not. The documents may come from teaching and research institutions in France or abroad, or from public or private research centers.

L'archive ouverte pluridisciplinaire **HAL**, est destinée au dépôt et à la diffusion de documents scientifiques de niveau recherche, publiés ou non, émanant des établissements d'enseignement et de recherche français ou étrangers, des laboratoires publics ou privés.

Boundary conditions at fluid porous interfaces

Christian Ruyer-Quil¹, Sanghasri Mukhopadhyay², and R Usha³

¹Université Savoie Mont Blanc, CNRS, LOCIE, 73000 Chambéry, France

²TDepartment of Mathematics, School of Advanced Sciences, Vellore Institute of Technology, Vellore 632014, Tamil Nadu, India

³Department of Mathematics, IIT Madras, Chennai, 600036 Tamil Nadu, India.

Abstract

We derive boundary conditions at the interface of a homogeneous and isotropic porous medium and an overlying fluid layer by averaging the generalized transport equations in the interfacial region and rewriting the obtained jump conditions at the effective sharp interface dividing the homogeneous fluid and porous layers, thus taking into account the thickness of the diffuse interface. We obtained jump boundary conditions in terms of geometrical parameters, namely the Brinkman penetration depth δ_B , the ratio $a = \Delta/\delta_B$ of the thickness of the interfacial region to the Brinkman depth, and the location of the effective dividing interface. This is the first attempt to determine the appropriate location of the dividing interface by matching the solutions to the one-domain and two-domain approaches. Jump boundary conditions reduce to the slip-transpiration-resistance model proposed by Lācis *et al.* [29], either in the thick interface limit ($e^a \gg 1$) or if the Darcy law is assumed to apply in the porous medium. In these limits, adequate choice of the dividing interface location enables to replace the slip condition by the continuity of the tangential velocity, yielding a simpler Dirichlet-transpiration-resistance model. Our formulation has the advantage that the effective coefficients depend explicitly on geometrical parameters that are easy to estimate in practice and, therefore, can be easily implemented. Numerical tests for parallel and non-parallel flows using the obtained boundary conditions or the generalized transport equations show excellent agreement. Our results can be easily extended to deal with 3D configurations and anisotropic porous media.

Keywords: porous media, flow-structure interaction

1 Introduction

One of the long-standing sources of challenging problems for mathematical analysis is the description and modelling of transport phenomena of a fluid in a porous medium and the transitional region at a fluid-porous interface responsible for mass and momentum transfer. The necessity for addressing this problem stems not only from the significant influence exerted by the presence of small-scale surface inhomogeneities at the interface on the transport phenomena but also from its ubiquitous occurrence in nature (benthic boundary layer, turbulent flow in the forest or urban location, flows over gravel stream beds, contaminant transport in rivers or atmosphere) and in many industrial and environmental applications (dendritic solidification of multicomponent mixtures, oil recovery, flow in heat exchangers, fuel cell and separation processes, in nuclear reactor vessels, in nuclear waste repositories), see, e.g., Alazmi & Vafai [1], Angot *et al.* [4], Bottaro [7], Gavrilov *et al.* [16], Lyubimova *et al.* [33]. Starting from the pioneering study by Beavers & Joseph [6] who considered a Poiseuille flow over a permeable medium employing an empirical slip boundary condition, referred to as the Beavers and Joseph (B-J) condition, where the governing equations in the two regions (Stokes and the Darcy equations) which model the dynamics are of different differential orders, there have been several theoretical and experimental efforts in the past few decades (see Angot *et al.* [3] for details). These studies have provided different models describing the dynamics to be employed in the two regions, depending on the phenomenon to be examined, namely Darcy, Forchheimer, or Darcy-Brinkman models, and the appropriate boundary conditions needed to connect the transport models in the two regions, so that one can investigate the dynamics in the whole region, determine and quantify the role

44 of the interfacial region. The B-J jump condition contains a dimensionless slip coefficient that depends
45 on the microstructure of the interfacial region [6, 17, 36, 40, 43, 45, 49, 50, 54]. Note that the transition
46 region is one in which the flow velocity in the fluid layer reduces drastically until it reaches an average
47 seepage velocity that the Darcy equation can predict. It is crucial to examine the general form of the
48 admissible boundary conditions from a mathematical point of view, given the models in the fluid and the
49 porous regions. It is also important to characterize the transfer in the transition region (mass, momentum)
50 and to model these by appropriate boundary conditions.

51 From a macroscopic perspective (where the concept of interface is related to the average representa-
52 tion), the fluid flow in a coupled flow system has been characterized by two modelling approaches, the
53 One-Domain Approach (ODA) and the Two-Domain Approach (TDA), which employ volume-averaging
54 techniques that provide a framework for obtaining macroscopic models from point-wise models at fluid
55 and porous medium scales [49].

56 The ODA considers the system as a continuum, where the geometrical properties (porosity, permeabil-
57 ity) and transport phenomena display rapid spatial changes in the inter-region [17, 36, 46, 49, 50], regarded
58 as a thin transition porous layer (see figure 1 a). The earlier attempts to describe the transport governed by
59 the generalized transport equations (GTE), valid everywhere in the entire system, have employed heuristic
60 expressions for permeability, but the predictions near the interface have not been satisfactory [14, 25].
61 This suggested a need for accounting for the correct spatial dependence of permeability everywhere in
62 the system through the GTE and for understanding how the spatial variations of the effective coefficients
63 are related to the size of the averaging volume employed to derive the macroscopic equations. The sub-
64 sequent efforts to fulfil the above requirements are based on GTE formulations, which are free of length
65 constraints, and they accounted for porosity variations by including first and second Brinkman correction
66 terms [39, 48]. There were suggestions to neglect the second Brinkman correction term [11, 12, 13] as its
67 contribution is considered through the other terms in the GTE. However, the inclusion of these terms has
68 also been accepted as it can be regarded just as a result of the up-scaling method employed to derive the
69 macroscopic equations.

70 Motivated by the relevance of the derivation of a reliable GTE that accurately describes the momen-
71 tum transport across fluid-porous medium, Hernandez-Rodriguez *et al.* [20] have presented a momentum
72 GTE (ODA approach), valid everywhere in the system and expressed in terms of position-dependent effec-
73 tive medium coefficients, containing the two Brinkman corrective terms along with the Darcy term. The
74 ODA predictions compare well with the results generated by averaging the local profiles resulting from
75 pore-scale simulations. They have predicted the position-dependent permeability tensor from both pore-
76 scale simulations and the solution of the corresponding local closure problem in a typical domain of the
77 fluid-porous medium boundary. Their analysis reveals that including the first and the second Brinkman
78 correction terms, along with the position-dependent intrinsic permeability tensor in the Darcy term in the
79 GTE for momentum transport, facilitates accurate predictions of the average velocity profiles everywhere
80 in the system. It is worth mentioning that the derivation of the GTE for momentum transport also gains
81 significance in the context of TDA since one can assess whether or not the inclusion of additional terms
82 helps in the accurate prediction of the associated jump coefficients and the position of the dividing surface.

83 The TDA considers the porous medium-fluid region as two continuous regions separated by a dividing
84 surface (see figure 1 b). Different models for the fluid and the porous medium scales have been imple-
85 mented and matched through the corresponding developed jump conditions at the dividing surface [51, 52].
86 The solution of the associated closure problems has supplied the coefficients involved in the jump condi-
87 tions. There have been continued efforts in proposing adequate boundary conditions at the interface of
88 the two domains, but there are certain features of the momentum and the mass transport phenomena that
89 have not been accounted for, resulting in some failure to capture significant physical characteristics of the
90 porous surface. The derivation of the boundary conditions must incorporate a direct correlation between
91 the microscopic geometrical details of the porous medium and the corresponding macroscopic transport of
92 mass and momentum; this being a complicated effort in such multi-scale problems, an effective approach
93 has been proposed to capture the averaged effect of the microscale characteristics on the macroscopic pro-
94 cesses within the framework of TDA. This corresponds to imposing the boundary conditions at a fictive
95 interface between the free fluid and the porous region. Note that the jump boundary conditions are a result
96 of the integration of the momentum transport over a thin transition layer of the ODA [19, 47].

97 The investigations devoted to the derivation of the jump boundary conditions for inertia-less, one-

98 dimensional channel flow parallel to the porous layer [6, 9, 19, 26, 34, 39, 42, 47], for general two or three-
99 dimensional inertia-less viscous flow and arbitrary flow direction at the interface [3], employing asymptotic
100 modelling [2], for inertial flow through a permeable interface [37], for multidimensional arbitrary flow
101 direction and for macroscopic scale for one-dimensional (1D) channel flow [22, 43], at the pore scale
102 for 1D channel flow [5, 8, 28, 32, 41, 53, 55], reveal that the jump boundary conditions represent the
103 integration of transport phenomena over the transition layer. The derived jump boundary conditions based
104 on the combination of the ODA and the TDA approaches have either assumed the volume averaging method
105 [38, 39], or are based on the solution of an ancillary closure problem related to macroscopic deviations [47],
106 or used matched asymptotic expansion [13], or asymptotic analysis [3].

107 In the above investigations, the normal free-flow velocity v^f is either set to zero at the interface (while
108 modelling a porous surface with very small permeability by a rigid surface with wall slip, characterized
109 by a slip length) or to the velocity in the porous medium justified by conservation of mass arguments or
110 leading order boundary condition [27, 30, 35]. However, the mass transfer to the exterior fluid takes place
111 due to stream-wise variation of the slip velocity across a depth below the interface where wall-normal
112 velocity exists and is non-zero. Hence, the boundary condition on the wall-normal velocity at the interface
113 must be a relation connecting v^f , the Darcy seepage velocity v^p , and the amount of exchange of mass that
114 the porous medium permits across the interface.

115 Further, the free fluid pressure p^f is assumed to be continuous across the interface and is the same
116 as the pressure in the porous medium (p^p , the pore pressure) in contrast to the theoretical and numerical
117 predictions [24, 28, 31] which revealed that there is a jump in pressure: $p^f - p^p = 2\mu v_y$; μ is the dynamic
118 viscosity of the fluid. Note that $v_y = 0$ stands only for parallel flows and that there are systems (non-
119 parallel flows) such as the turbulent channel flow [29, 54] in which the wall-normal velocity fluctuations
120 contribute to the friction at a rough/porous wall. [29] thus proposed to introduce a resistance coefficient
121 which quantifies the friction induced by the crossing of the interface, as well as a transpiration length which
122 represents the distance from the interface below which the normal velocity differs from the seepage Darcy
123 one.

124 In such scenarios, one has to account for not only the transport of the interface tangential momentum
125 but also that of mass and interface normal momentum. Hence, the pressure boundary condition must
126 relate the normal stress of the free fluid flow on the interface, taking into consideration that $v_y \neq 0$ and the
127 contribution of the frictional force generated by the Darcy seepage velocity v^p in the normal stress from
128 the porous medium. The idea is to derive a boundary condition with a flow direction that is neither normal
129 nor tangential to the porous fluid interface and besides is evolving in the tangential direction ($v_y \neq 0$).

130 The above-mentioned investigations and arguments demonstrate that the description of the transport
131 phenomena across the transition region must accurately account for the dependence of the exchange of
132 mass, momentum, energy, and other passive scalars on the inhomogeneities at the interface between the
133 free-flowing fluid and the porous medium and that, for the given physical phenomena, the precise loca-
134 tion of the interface inside the fluid-porous transitional region may have a significant impact on the final
135 result. This suggests that it is important to propose the exact location of the interface and the appropriate
136 boundary conditions at a sharp interface within the interfacial region, taking into account the thickness of
137 the transitional region. The above requirement is also supported by experimental observations on transition
138 layer thickness at a fluid, porous interface in packed beds by [17]. The thickness 2Δ of the transition zone
139 (height below the permeable interface up to which the velocity decreases to the Darcy seepage velocity)
140 has been shown to be of the order of the grain diameter and hence much larger than the square root of the
141 permeability.

142 This calls for the derivation of appropriate boundary conditions at a sharp interface within the tran-
143 sitional region of the thickness of order 2Δ , i.e. of the order of the grain diameter, employing accurate
144 quadrature rules to evaluate the integrals involved in the computations. In view of the above, the present
145 study considers the derivation of the jump boundary conditions at a fluid-porous medium interface (TDA),
146 taking into account the transitional layer thickness and integrating the ODA governing equations across the
147 diffuse interface employing consistent quadrature rules [3].

148 In our geometrical argument, we take into account the following two effects within the TDA: (i) the
149 effect of the transition between the fluid and the porous region and (ii) the Brinkman diffusion within the
150 bulk of the porous medium. Note that if the Brinkman sub-layer, defined as the region of the flow where
151 Brinkman diffusive terms are non-negligible, is included within the interfacial region, it makes no sense

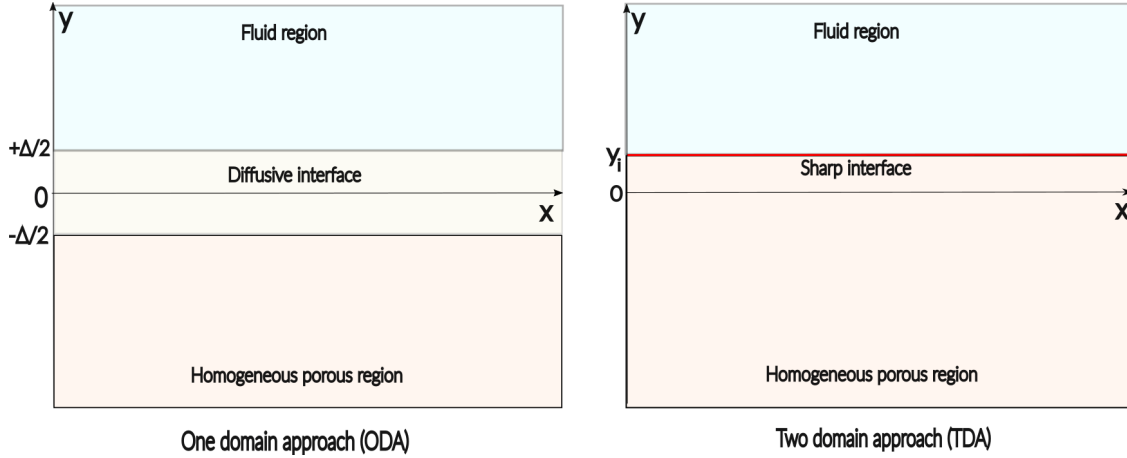


Figure 1: Sketches of the interfacial fluid-porous interfacial region modelled by the ODA, TDA approaches.

152 to include Brinkman corrections in the bulk of the porous medium within the framework of TDA. Thus,
 153 it is more appropriate to use the Darcy approximation of the porous flow coupled with the jump boundary
 154 conditions. In this regard, we have identified two parameters that characterize the interfacial region, namely,
 155 the thickness of the interfacial region, Δ and the ratio $a = \Delta/\delta_B$ of interfacial thickness to the Brinkman
 156 penetration depth δ_B (the depth below which the Brinkman diffusive terms are dominant), and propose to
 157 present the appropriate boundary conditions for the TDA. We have obtained sets of boundary conditions
 158 that are expressed explicitly in terms of these two parameters, in contrast to the previous attempts where
 159 the coefficients in the boundary conditions are given in terms of the integrals of the pore-scale variables.

160 The paper is organized as follows: Section 2 presents the mathematical description of the proposed
 161 model and the derivation of the effective homogenized boundary conditions, with coefficients expressed
 162 explicitly in terms of the three relevant parameters introduced. The proposed TDA model is validated for
 163 channel flow and stagnation point flow over a porous wall with the suction flow in section 3, and section 4
 164 presents the concluding remarks.

165 2 Mathematical modelling

166 We consider a system comprising fluid and porous regions separated by a planar diffuse interface at $y = 0$,
 167 of thickness 2Δ . The porous bed is isotropic and homogeneous, i.e., the permeability and porosity in the
 168 bulk of the porous region are assumed constant, κ_H and ε_H , and to vary continuously as functions $\kappa(y)$
 169 and $\varepsilon(y)$ within the diffuse interfacial region. Fundamental properties of the fluid, density (ρ) and dynamic
 170 viscosity (μ) are considered to remain constant. The kinematic viscosity is denoted by $\nu = \mu/\rho$. For ease
 171 of simplicity, we limit ourselves to considering a two-dimensional (2D) flow, though the analysis can be
 172 generalized to 3D flows without difficulty.

173 Within the one-domain approach (ODA) (for details see Hernandez-Rodriguez *et al.* [20], Hirata *et al.*
 174 [23]), the flow is governed by the equations

$$\begin{aligned} \nabla \cdot \mathbf{v} &= 0, & (1a) \\ \frac{Re}{\varepsilon} \left[\mathbf{v}_t + \nabla \cdot \left(\frac{1}{\varepsilon} \mathbf{v} \otimes \mathbf{v} \right) \right] &= -\nabla p + \frac{1}{\varepsilon} \Delta \mathbf{v} - \frac{1}{\kappa} \mathbf{v} - \frac{1}{\varepsilon} \nabla \varepsilon \cdot \nabla \left(\frac{\mathbf{v}}{\varepsilon} \right). & (1b) \end{aligned}$$

175 where subscripts denote partial derivatives. Body forces, such as gravity, are here assumed to derive from a
 176 potential and are included in the definition of the pressure field. The last terms $-\varepsilon^{-1} \nabla \varepsilon \cdot \nabla (\varepsilon^{-1} \mathbf{v})$ are the
 177 second Brinkman corrections, which are non-zero only in the diffuse interfacial regions where the porosity
 178 gradients cannot be a priori neglected. However, these terms are generally considered to be weak, though
 179 Hernandez-Rodriguez *et al.* [20] have shown that they must be retained in order to capture precisely the

180 velocity profile of parallel flows. As shown later on in this work, these terms affect only weakly the base
 181 flow profile. We will therefore neglect them in our analysis of the interfacial region.

182 The governing equations have been made dimensionless using characteristic length \bar{L} and velocity
 183 \bar{U} scales, e.g. the total thickness of the entire continuum and the averaged velocity of the fluid. The
 184 pressure scale is equal to $\mu\bar{U}/\bar{L}$. Three dimensionless groups characterize the flow, namely the Reynolds
 185 number $Re = \bar{U}\bar{L}/\nu$, the Darcy number $Da = \kappa_H/\bar{L}^2$ and the dimensionless thickness of the interfacial
 186 region $\Delta = \bar{\Delta}/\bar{L}$.

187 In contrast, within the two-domain approach (TDA), the porous and fluid domains are separated by
 188 a sharp interface of zero thickness, the fluid and porous regions being homogeneous. Within TDA, the
 189 location y_i of the sharp interface dividing the fluid and porous regions can be chosen arbitrarily within
 190 the interfacial region, i.e. $-\Delta < y_i < \Delta$. The solution to the TDA, labelled with l and p superscripts, is
 191 governed by the Navier-Stokes equation in the liquid phase

$$\nabla \cdot \mathbf{v}^l = 0, \quad Re \left[\mathbf{v}_t^l + \nabla \cdot (\mathbf{v}^l \otimes \mathbf{v}^l) \right] = -\nabla p^l + \Delta \mathbf{v}^l, \quad (2)$$

192 and the Darcy-Brinkman equations

$$\nabla \cdot \mathbf{v}^p = 0, \quad 0 = -\nabla p^p + \frac{1}{\varepsilon_H} \Delta \mathbf{v}^p - \frac{1}{Da} \mathbf{v}^p, \quad (3)$$

193 or the Darcy equations

$$\nabla \cdot \mathbf{v}^p = 0, \quad 0 = -\nabla p^p - \frac{1}{Da} \mathbf{v}^p, \quad (4)$$

194 if the first Brinkman correction is neglected or not in the porous phase.

195 2.1 Interfacial jump conditions

196 Following [3], we integrate the ODA governing equations (1) across the diffuse interfacial region in order
 197 to obtain jump conditions connecting the fluid and porous layers. We introduce the scale $\delta_B = \sqrt{Da}/\varepsilon_H$
 198 below which Brinkman diffusive terms are dominant in the bulk of the porous medium. We will thus refer
 199 to δ_B as a Brinkman penetration depth.

200 Noteworthy is that our definition of the Brinkman penetration depth differs from the thickness of the
 201 Brinkman boundary layer, which we denote here by Δ_B , as identified by Hernandez-Rodriguez *et al.* [21]
 202 as the typical distance over which the velocity profile decreases drastically from the velocity at the surface
 203 of the porous medium to the Darcy seepage velocity. These authors have shown that the extension of this
 204 boundary layer is of the order of the size r_0 of the averaging volume in the homogenization method, which
 205 also corresponds to the typical extension of the variations of the permeability distribution obtained by the
 206 same method [20]. Thus $\Delta_B = O(\Delta)$, and may be much larger than the Brinkman penetration depth δ_B in
 207 their computations. We thus infer that the Brinkman boundary layer has a thickness Δ_B of the order of the
 208 maximum of δ_B and Δ .

209 As the interfacial region is thin in comparison to the macro scale, we stretch the normal coordinate as
 210 $Y = y/\Delta$. The continuity equation thus reads

$$\Delta u_x + v_Y = 0 \quad (5)$$

211 Since $u_x = O(1)$ and, in the bulk of the porous region, the velocity is governed by the Darcy law, i.e.
 212 $v = O(Da) = O(\delta_B^2) = O(\Delta^2/a^2)$, we conclude that $v = O(\Delta)$ in the interfacial region. We thus rescale the
 213 normal velocity component such that $V = v/\Delta$.

214 The governing equations (1) then read

$$V_Y = -u_x, \quad (6a)$$

$$\frac{1}{\varepsilon} u_{YY} - \Delta^2 \frac{u}{\kappa} = \Delta^2 \frac{Re}{\varepsilon} \left[u_t + \left(\frac{u^2}{\varepsilon} \right)_x + \left(\frac{uV}{\varepsilon} \right)_Y \right] + \Delta^2 p_x - \frac{\Delta^2}{\varepsilon} u_{xx}, \quad (6b)$$

$$\frac{1}{\varepsilon} V_{YY} - \Delta^2 \frac{V}{\kappa} = \Delta^2 \frac{Re}{\varepsilon} \left[V_t + \left(\frac{uV}{\varepsilon} \right)_x + \left(\frac{V^2}{\varepsilon} \right)_Y \right] + p_Y - \frac{\Delta^2}{\varepsilon} V_{xx}, \quad (6c)$$

215 where $\Delta^2/\kappa = O(1)$. Truncating at order Δ , we obtain a set of equations that we rewrite with the original
 216 scales

$$v_y = -u_x, \quad (7a)$$

$$\frac{1}{\varepsilon} u_{yy} - \frac{u}{\kappa} = 0, \quad (7b)$$

$$\frac{1}{\varepsilon} v_{yy} - \frac{v}{\kappa} = p_y \quad (7c)$$

217 Thus, at the leading order, inertia is negligible in the interfacial region. The pressure gradient is oriented
 218 orthogonally to the interface and drives a flow in the normal direction.

219 Following [3], we integrate (7) using the trapezoidal quadrature rule

$$\int_a^b f(x) dx = \frac{h}{2} [f(a) + f(b)] + O \left[\max_{x \in [a,b]} |f''(x)| h^3 \right] \quad (8)$$

220 where $h = b - a$, and the quadrature of the integral of products

$$\int_a^b f(x) g(x) dx = \frac{1}{h} \int_a^b f(x) dx \int_a^b g(x) dx + O \left[\max_{x \in [a,b]} |g'(x)| \langle |g| \rangle h^2 \right], \quad (9)$$

221 with $\langle |g| \rangle = h^{-1} \int_a^b |g| dx$.

222 Therefore, integration of the continuity equation (7a) gives

$$v|_{\Delta} - v|_{-\Delta} = - \int_{-\Delta}^{\Delta} u_x dy \approx -\Delta (u_x|_{\Delta} + u_x|_{-\Delta}) = \Delta (v_y|_{\Delta} + v_y|_{-\Delta}), \quad (10)$$

223 Similarly, we have

$$\int_{-\Delta}^{\Delta} \frac{1}{\varepsilon} u_{yy} dy \approx \frac{1}{2\Delta} \int_{-\Delta}^{\Delta} \frac{1}{\varepsilon} dy \int_{-\Delta}^{\Delta} u_{yy} dy \approx \frac{1}{2} \left(1 + \frac{1}{\varepsilon_H} \right) (u_y|_{\Delta} - u_y|_{-\Delta}) \quad (11)$$

224 and

$$\int_{-\Delta}^{\Delta} \frac{u}{\kappa} dy \approx \Delta \left(\frac{u}{\kappa} \Big|_{y=-\Delta} + \frac{u}{\kappa} \Big|_{y=\Delta} \right) \approx \frac{\Delta}{Da} u|_{-\Delta} \quad (12)$$

225 We thus obtain

$$\frac{1 + \varepsilon_H}{2\varepsilon_H} (u_y|_{\Delta} - u_y|_{-\Delta}) = \frac{\Delta}{Da} u|_{-\Delta}, \quad (13)$$

226 We next integrate the normal momentum balance (7c) to obtain

$$p|_{\Delta} - p|_{-\Delta} = \frac{1 + \varepsilon_H}{2\varepsilon_H} (v_y|_{\Delta} - v_y|_{-\Delta}) - \frac{\Delta}{Da} v|_{-\Delta}, \quad (14)$$

227 To complete our system of jump conditions connecting the fluid and porous layers, we need to write a
 228 relation between the jump of velocity and the shear stress. Still following [3], we write

$$\int_{-\Delta}^{\Delta} \frac{1}{\varepsilon} u_y dy \approx \frac{1}{2\Delta} \int_{-\Delta}^{\Delta} \frac{1}{\varepsilon} dy \int_{-\Delta}^{\Delta} u_y dy \quad (15)$$

229 Applying the trapezoidal rule (8) on each side of this equation gives

$$\frac{1 + \varepsilon_H}{2\varepsilon_H} (u|_{\Delta} - u|_{-\Delta}) = \Delta \left(u_y|_{\Delta} + \frac{1}{\varepsilon_H} u_y|_{-\Delta} \right) \quad (16)$$

230 Let us stress that we have computed the integrals $\int_{-\Delta}^{\Delta} u/\kappa dy$ and $\int_{-\Delta}^{\Delta} v/\kappa dy$ using the trapezoidal rule (8)
 231 instead of the quadrature rule (9) employed by Angot *et al.* [3]. As discussed in the appendix A, using (9)
 232 leads to $u|_{\Delta} = O(\Delta) \ll 1$, which erroneously implies that the fluid layer essentially sees a no-slip boundary

233 condition at the top of the interfacial region and therefore that the extension of the Brinkman boundary
 234 layer is negligible. We note that, contrary to (58a), the jump of the tangential shear stress (13) is naturally
 235 balanced as $u_y|_{\Delta} - u_y|_{-\Delta} = O(\Delta)$ and $u|_{-\Delta} = O(Da/\varepsilon_H)$ since the flow in the bulk of the porous medium is
 236 essentially governed by the Darcy law.

237 In order to obtain a set of symmetrical jump relations for the tangential and normal velocities, we
 238 rewrite the normal velocity jump by evaluating the integral $\int_{-\Delta}^{\Delta} v_y/\varepsilon dy$, which gives

$$\frac{1 + \varepsilon_H}{2\varepsilon_H} (v|_{\Delta} - v|_{-\Delta}) = \Delta \left(v_y|_{\Delta} + \frac{1}{\varepsilon_H} v_y|_{-\Delta} \right) \quad (17)$$

239 Finally, we write a jump relation for the gradient of pressure that will be used to close the system of
 240 equations for the boundary conditions that we will derive in the next section. Taking the divergence of the
 241 momentum balance gives

$$p_{yy} = v_{yy} \frac{d}{dy} \left(\frac{1}{\varepsilon} \right) - v \frac{d}{dy} \left(\frac{1}{\kappa} \right) \quad (18)$$

242 which we integrate across the interfacial region as

$$\int_{-\Delta}^{\Delta} p_{yy} dy = \left[\frac{d}{dy} \left(\frac{1}{\varepsilon} \right) v_y - \frac{v}{\kappa} \right]_{-\Delta}^{\Delta} - \int_{-\Delta}^{\Delta} \frac{d^2}{dy^2} \left(\frac{1}{\varepsilon} \right) v_y - \frac{1}{\kappa} v_y dy \quad (19)$$

243 which gives

$$p_y|_{\Delta} - p_y|_{-\Delta} = \frac{1}{Da} (v|_{-\Delta} - \Delta v_y|_{-\Delta}) \quad (20)$$

244 which, with the help of (7c), can also be rewritten as

$$v_{yy}|_{\Delta} - \frac{1}{\varepsilon_H} v_{yy}|_{-\Delta} = -\frac{\Delta}{Da} v_y|_{-\Delta} \quad (21)$$

245 Next, we integrate v_{yy}/ε to get

$$\frac{1 + \varepsilon_H}{2\varepsilon_H} (v_y|_{\Delta} - v_y|_{-\Delta}) = \Delta \left(v_{yy}|_{\Delta} + \frac{1}{\varepsilon_H} v_{yy}|_{-\Delta} \right). \quad (22)$$

246 The jump relations (21) and (22) will be used to eliminate the second derivatives of the normal velocity v
 247 and close our set of boundary equations as discussed in the next section.

248 The set of four jump conditions (13), (16), (14) and (17), is similar to the one derived by [3]. However,
 249 these authors postulated u_x to be negligible, and thus also v_y , and therefore found the normal velocity to be
 250 continuous within the interfacial region instead of the jump condition (17).

251 2.2 Two-domain approach boundary conditions

252 In this section, we propose to derive from the jump conditions (13), (14), (16), (17), (21) and (22), boundary
 253 conditions for the two-domain approach (TDA). We assume that the solution to the TDA, labelled with l
 254 and p superscripts to denote the fluid and porous regions, coincides with the ODA solution outside the
 255 diffuse interface. Similarly to section 2.1, considering the diffuse interface to be thin, a boundary-layer
 256 analysis gives at leading order

$$v_y^p = -u_x^p, \quad \frac{1}{\varepsilon_H} u_{yy}^p - \frac{u^p}{Da} = 0, \quad \frac{1}{\varepsilon_H} v_{yy}^p - \frac{v^p}{Da} - p_y^p = 0, \quad (23a)$$

$$v_y^l = -u_x^l, \quad u_{yy}^l = 0, \quad v_{yy}^l - p_y^l = 0. \quad (23b)$$

257 Taking the divergence of the momentum balances gives Laplace equations for the pressure field, i.e.

$$p_{yy}^l = 0, \quad p_{yy}^p = 0, \quad (24)$$

258 from which we deduce that the pressure gradients p_y^l and p_y^p are independent of y at leading order within
 259 the interfacial region. Matching with the outer regions thus ensures that p_y^l and p_y^p are $O(1)$ quantities
 260 and therefore, $v^p = O(\Delta^2)$, $v_y^p = O(\Delta)$, $v_{yy}^p = O(1)$, $v^l = O(\Delta^2)$, $v_y^l = O(\Delta)$ and $v_{yy}^l = O(1)$. Consequently,
 261 the continuity equations provide the estimates $u^p = O(\Delta)$, $u_y^p = O(1)$, $u^l = O(\Delta)$, $u_y^l = O(1)$ within the
 262 interfacial region. These ordering relations will be used to discuss the boundary conditions which we
 263 propose below.

264 From (23), the tangential velocity component can easily be integrated to give

$$u^p = u^p|_i \cosh \frac{y-y_i}{\delta_B} + \delta_B u_y^p|_i \sinh \frac{y-y_i}{\delta_B}, \quad u^l = u^l|_i + (y-y_i) u_y^l|_i \quad (25a)$$

265 From which the normal velocity component can be obtained with the help of the continuity equation

$$v^p = v^p|_i + v_y^p|_i \delta_B \sinh \frac{y-y_i}{\delta_B} + v_{yy}^p|_i \delta_B^2 \left[\cosh \frac{y-y_i}{\delta_B} - 1 \right], \quad v^l = v^l|_i + (y-y_i) v_y^l|_i + \frac{(y-y_i)^2}{2} v_{yy}^l|_i, \quad (25b)$$

266 and the pressure distribution

$$p^p = p^p|_i + (y-y_i) \left(\frac{1}{\varepsilon_H} v_{yy}^p|_i - \frac{v^p|_i}{Da} \right), \quad p^l = p^l|_i + (y-y_i) v_{yy}^l|_i \quad (25c)$$

267 Substitution of (25) into (13) and (16) leads to the following boundary conditions expressed at the sharp
 268 interface $y = y_i$:

$$p^l|_i - p^p|_i = \frac{\xi}{\delta_B \varepsilon_H} v^p|_i + \frac{1 + \varepsilon_H}{2 \varepsilon_H} v_y^l|_i - \alpha v_y^p|_i + (\xi + \gamma) \delta_B v_{yy}^l|_i + \left(\beta - \frac{\xi}{\varepsilon_H} \right) \delta_B v_{yy}^p|_i, \quad (26a)$$

$$\frac{1 + \varepsilon_H}{2 \varepsilon_H} u_y^l|_i - \alpha u_y^p|_i = -\frac{\beta}{\delta_B} u^p|_i, \quad (26b)$$

$$\frac{1 + \varepsilon_H}{2 \varepsilon_H} u^l|_i - \alpha u^p|_i = -\gamma \delta_B u_y^l|_i - \beta \delta_B u_y^p|_i, \quad (26c)$$

$$\frac{1 + \varepsilon_H}{2 \varepsilon_H} \left(v^l|_i - v^p|_i \right) = -\gamma \delta_B v_y^l|_i - \beta \delta_B v_y^p|_i + \zeta \delta_B^2 v_{yy}^l|_i + \delta_B^2 \left(\alpha - \frac{1 + \varepsilon_H}{2 \varepsilon_H} \right) v_{yy}^p|_i, \quad (26d)$$

$$v_{yy}^l|_i - \hat{\alpha} v_{yy}^p|_i = -\frac{\hat{\beta}}{\delta_B} v_y^p|_i, \quad (26e)$$

$$\frac{1 + \varepsilon_H}{2 \varepsilon_H} v_y^l|_i - \alpha v_y^p|_i = -\gamma \delta_B v_{yy}^l|_i - \beta \delta_B v_{yy}^p|_i, \quad (26f)$$

269 where $\xi = y_i/\delta_B$ and

$$\alpha = \frac{(1 + \varepsilon_H)C - 2aS}{2\varepsilon_H}, \quad \beta = \frac{(1 + \varepsilon_H)S - 2aC}{2\varepsilon_H}, \quad \gamma = \frac{(a - \xi)(1 - \varepsilon_H)}{2\varepsilon_H} - \xi, \quad (27a)$$

$$\zeta = \frac{(a - \xi)[\xi(1 + \varepsilon_H) + a(3\varepsilon_H - 1)]}{4\varepsilon_H}, \quad (27b)$$

$$\hat{\alpha} = \frac{C + aS}{\varepsilon_H}, \quad \hat{\beta} = \frac{S + aC}{\varepsilon_H}, \quad (27c)$$

$$C = \cosh(a + \xi), \quad S = \sinh(a + \xi), \quad \text{and} \quad a = \Delta/\delta_B. \quad (27d)$$

270 Differentiating (26b) and (26c) with respect to x and adding them to (26d) and (26a) gives

$$p^l|_i - p^p|_i = \frac{\xi}{\delta_B \varepsilon_H} v^p|_i + \xi \delta_B \left(v_y^l|_i - \frac{1}{\varepsilon_H} v_{yy}^p|_i \right), \quad (28a)$$

$$\frac{1 + \varepsilon_H}{2 \varepsilon_H} \left(v^l|_i - v^p|_i \right) = -\gamma \delta_B v_y^l|_i + \delta_B^2 \left(\zeta + \frac{1 + \varepsilon_H}{2 \varepsilon_H} \right) v_y^l|_i - \delta_B^2 \frac{1 + \varepsilon_H}{2 \varepsilon_H} v_{yy}^p|_i \quad (28b)$$

271 Combining (26e) and (26f) enables to eliminate $v_{yy}^l|_i$ and $v_{yy}^p|_i$, which leads to the boundary conditions

$$p^l|_i - p^p|_i = \frac{\xi}{\delta_B \varepsilon_H} v^p|_i - \xi \left(\phi v_y^l|_i + \psi v_y^p|_i \right), \quad (29a)$$

$$\frac{1 + \varepsilon_H}{2\varepsilon_H} u_y^l|_i - \alpha u_y^p|_i = -\frac{\beta}{\delta_B} u^p|_i, \quad (29b)$$

$$\frac{1 + \varepsilon_H}{2\varepsilon_H} u^l|_i - \alpha u^p|_i = -\gamma \delta_B u_y^l|_i - \beta \delta_B u_y^p|_i, \quad (29c)$$

$$v^l|_i - v^p|_i = -\hat{\phi} \delta_B v_y^l|_i - \hat{\psi} \delta_B v_y^p|_i. \quad (29d)$$

272 where

$$\phi = \frac{(1 + \varepsilon_H)(\hat{\alpha} \varepsilon_H - 1)}{2\varepsilon_H^2(\beta + \hat{\alpha} \gamma)}, \quad (30a)$$

$$\psi = \frac{\alpha(1 - \hat{\alpha} \varepsilon_H) + \hat{\beta}(\beta \varepsilon_H + \gamma)}{\varepsilon_H(\beta + \hat{\alpha} \gamma)}, \quad (30b)$$

$$\hat{\phi} = \frac{\hat{\alpha} - (1 + \varepsilon_H)^2 + 4\beta \varepsilon_H^2 \gamma + \hat{\alpha} \varepsilon_H [2 + \varepsilon_H + 4\varepsilon_H \gamma^2 + 2(1 + \varepsilon_H)\zeta]}{2\varepsilon_H(1 + \varepsilon_H)(\beta + \gamma \hat{\alpha})}, \quad (30c)$$

$$\hat{\psi} = \frac{(1 + \varepsilon_H)[\alpha(1 - \hat{\alpha}) + (\beta + \gamma)\hat{\beta}] + 2(\beta \hat{\beta} - \alpha \hat{\alpha})\varepsilon_H \zeta}{(1 + \varepsilon_H)(\beta + \gamma \hat{\alpha})} \quad (30d)$$

273 Conditions (29c) and (29d) represent the jump of velocity induced by the shear rate in the interfacial
 274 region. (29a) corresponds to the jump of pressure generated by the balance of normal stresses at the
 275 interface. Finally, (29b) accounts for the friction exerted by the porous medium on the flow in the interfacial
 276 region, which is responsible for a jump in tangential shear rate.

277 From (29a), we obtain that, at the leading order, the pressure is continuous if the sharp interface is
 278 chosen to correspond to the middle of the diffuse interfacial region ($\xi = 0$). This result is consistent with
 279 the pore-scale simulations of a fluid-porous interface performed by Carraro *et al.* [10] for an isotropic
 280 porous medium. However, the coefficients of the boundary conditions (29) are dependent on the choice
 281 of location of the dividing sharp interface through the parameter ξ . This calls for the best choice of that
 282 parameter, which enables to obtain the best agreement between ODA and TDA solutions. Finding the best
 283 value for ξ has no clear answer. However, since tangential velocities u^l and u^p are $O(\Delta)$ in the interfacial
 284 region, whereas the normal velocities are $O(\Delta^2)$, it is convenient to look for the value of ξ based on the
 285 tangential velocity profiles.

286 The Darcy seepage velocity being small, we propose to adjust ξ in order to set $u^l|_i$ to zero, or close
 287 to zero, so that $u^p|_i \approx u^l|_i$. Because of the exponential nature of the solution (25), we have $u^p|_i \approx \delta_B u_y^p|_i$.
 288 Thus, setting $u^p|_i = \delta_B u_y^p|_i$ and $u^l|_i$ into the velocity and shear stress boundary conditions (29c) and (29b)
 289 yield

$$(1 + \varepsilon_H - 2\varepsilon_H \gamma) u_y^l|_i = 0 \quad (31)$$

290 Since $u_y^l|_i \neq 0$, we obtain a condition for the location of the sharp interface, namely

$$\xi = \frac{a(1 - \varepsilon_H) - 1 - \varepsilon_H}{1 + \varepsilon_H}, \quad (32)$$

291 The condition $\xi > -a$ implies $a > (1 + \varepsilon_H)/2$. Thus, (32) will be employed only for $a > (1 + \varepsilon_H)/2$
 292 to guarantee a location of the sharp dividing interface within the interfacial region. In the case of a thin
 293 interfacial region, for which $a < (1 + \varepsilon_H)/2$, the sharp dividing interface is placed at the middle of the
 294 interfacial region ($\xi = 0$).

295 2.3 Thick interface limit

296 The thickness of the interfacial region is generally much larger than the Brinkman penetration depth, so
 297 the ratio $a = \Delta/\delta_B > 1$. This is justified by the experimental observations of Goharzadeh *et al.* [17]. Let

298 us thus consider the limit of a thick diffuse interface, i.e. $A = e^{-a} \ll 1$, $\cosh a \approx 1/(2A)$ and $\sinh a \approx$
 299 $1/(2A)$. Expanding the boundary conditions (29c) and (29b) for the tangential velocities and shear rates
 300 and truncating them at the leading order with respect to A give

$$u^p|_i = \delta_B u_y^p|_i, \quad (33a)$$

$$u^l|_i = -\delta_B \frac{(1 - \varepsilon_H)a + (1 + \varepsilon_H)(1 - \xi)}{1 + \varepsilon_H} u_y^l|_i, \quad (33b)$$

301 Therefore, in the case of a thick diffuse interface, a partial decoupling of the fluid and porous regions
 302 is observed as the shear rate at the sharp interface $y = y_i$ in the fluid (porous) region depends only on
 303 the velocity in the fluid (porous) region. (33b) is the slip boundary condition obtained by [42] using
 304 homogenization techniques, starting from the Darcy equations in the porous medium [26].

305 We note that $a \gg 1$ implies that the diffuse interface thickness 2Δ is much larger than the Brinkman
 306 penetration depth δ_B , which is the scale below which Brinkman diffusive terms are effective. Therefore,
 307 the Brinkman diffusion is inefficient at the scale Δ and the fluid region experiences a permeable boundary
 308 essentially governed by the Darcy law. Since scales smaller or of the order of Δ are not resolved in the
 309 TDA, accounting for the Brinkman diffusive terms in the homogeneous porous region in the limit of a
 310 thick diffuse interface makes little sense. Besides, for a thick interfacial region, the exponential nature of
 311 the solution to the Darcy-Brinkman equation leads to unrealistic values of u^p . Therefore, we assume a
 312 Darcy flow in the porous medium. Because of the degeneracy of the Darcy equation, the condition (33a)
 313 cannot be enforced in that case. Besides, for a Darcy flow, (24) implies that $v_y^p \approx 0$ in the interfacial region.
 314 We thus obtain

$$u^l|_i = Lu_y^l|_i, \quad (34a)$$

$$p^l|_i - p^p|_i = -Fv^p|_i + Gv_y^l|_i, \quad (34b)$$

$$v^l|_i - v^p|_i = Mv_y^l|_i. \quad (34c)$$

315 where

$$L = -\delta_B \frac{(1 - \varepsilon_H)a + (1 + \varepsilon_H)(1 - \xi)}{1 + \varepsilon_H}, \quad F = -\frac{\xi}{\delta_B \varepsilon_H}, \quad (35a)$$

$$G = \frac{\xi(1+a)(1 + \varepsilon_H)}{a^2(\varepsilon_H - 1) - (1 + \varepsilon_H)(\varepsilon_H - \xi) + a[\xi - 1 + \varepsilon_H(3 + \xi)]}, \quad (35b)$$

$$M = \delta_B \frac{M_A}{M_B}, \quad (35c)$$

$$M_A = a^3[-1 + (2 - 5\varepsilon_H)\varepsilon_H] + (1 + \varepsilon_H)^2(-2 + 2\varepsilon_H\xi - \xi^2) \\ + a(1 + \varepsilon_H)\{-2 + 2\varepsilon_H^2 - (\xi - 2)\xi - \varepsilon_H[4 + \xi(6 + \xi)]\} \\ + a^2\{-1 + 2\xi + \varepsilon_H[6 - \varepsilon_H(9 + 2\xi)]\}, \quad (35d)$$

$$M_B = 2(1 + \varepsilon_H)(a + a^2 + \varepsilon_H - 3a\varepsilon_H - a^2\varepsilon_H + \varepsilon_H^2 - (1 + a)(1 + \varepsilon_H)\xi). \quad (35e)$$

316 System (34) is similar to the model proposed by [29] to represent the interfacial momentum transfer at a
 317 rough or porous interface. Lācis et al. introduced a length, corresponding to the dimensionless coefficient
 318 M , which they call transpiration length, which represents the distance below which the normal velocity
 319 component differs from the Darcy seepage velocity. They also introduced a resistance coefficient F , which
 320 modelled the friction of the porous matrix on the flow in the normal direction. However, they assumed the
 321 shear stress in the fluid layer at the sharp interface to be equal to its value in the bulk of the flow, which
 322 corresponds to taking G equal to 2. Note that in our derivation, coefficients F and G are proportional to ξ .
 323 Hereinafter, we refer to (34) as the Slip-Transpiration-Resistance (STR) model.

324 The STR model (34) can be further simplified by conveniently choosing the location of the sharp
 325 interface such that to cancel out the slip length $L = 0$, which gives

$$\xi = \frac{1 + a + \varepsilon_H(1 - a)}{1 + \varepsilon_H}. \quad (36)$$

326 This choice leads to a no-slip boundary condition $u^l|_i = 0$, or more exactly to $u^l|_i = O(\Delta^2)$ as we solve the
 327 leading-order system of equations with respect to the expansion parameter Δ . Since the seepage velocity in
 328 the porous medium is $O(\Delta^2)$, we replace this no-slip condition with the continuity of the tangential velocity.
 329 Therefore, (34) is modified into

$$u^l|_i = u^p|_i, \quad (37a)$$

$$p^l|_i - p^p|_i = -Fv^p|_i + Gv_y^l|_i, \quad (37b)$$

$$v^l|_i - v^p|_i = Mv_y^l|_i, \quad (37c)$$

330 which we refer to hereinafter as the Dirichlet-Transpiration-Resistance (DTR) model. The resistance coef-
 331 ficient F , the transpiration dimensionless length M and the stress coefficient G are then given by

$$F = -\frac{\xi}{\delta_B \varepsilon_H} = -\frac{1 + a + \varepsilon_H(1 - a)}{\delta_B \varepsilon_H(1 + \varepsilon_H)}, \quad G = \frac{1 + \varepsilon_H + a[2 + a(1 - \varepsilon_H)]}{1 - \varepsilon_H^2 + a(1 + 3\varepsilon_H)}, \quad (38a)$$

$$M = \delta_B \frac{4a^2 \varepsilon_H^2(1 + a) - (1 + \varepsilon_H)^2(2\varepsilon_H - 3) + a(3 + 10\varepsilon_H + 7\varepsilon_H^2)}{2(1 + \varepsilon_H)[1 - \varepsilon_H^2 + a(1 + 3\varepsilon_H)]}. \quad (38b)$$

332 Let us underline that the no-slip boundary condition $u^l|_i = 0$ would have led to inconsistencies, as it
 333 implies that $v_y^l|_i = -u_x^l|_i = 0$. However, $v_y^l = O(\Delta^2)$ is of the same order of magnitude as $v^p|_i = O(\Delta^2)$ and
 334 must not be dropped out.

335 2.4 Two-domain approach boundary conditions for a Darcy flow

336 As stated above, the exponential nature of the solution to the TDA approach within the interfacial re-
 337 gion leads to unreasonable values of the tangential velocity in the vicinity of the sharp interface when the
 338 boundary conditions (29) are applied, i.e. whenever $a \gtrsim 2$ as will be shown in the next section. The condi-
 339 tions (37) can be employed along with the Darcy equation in the homogeneous porous medium but only if
 340 $e^a \gg 1$, which requires $a \gtrsim 5$. Another set of boundary conditions must be derived to bridge the gap in the
 341 range $2 \lesssim a \lesssim 5$.

342 A remedy for this drawback is to assume a Darcy flow within the homogeneous porous medium in the
 343 interfacial region. Thus, the leading-order equations for the TDA approach within the interfacial region
 344 become

$$v_y^p = -u_x^p, \quad \frac{u^p}{Da} = 0, \quad \frac{v^p}{Da} + p_y^p = 0. \quad (39)$$

345 which gives $u^p = 0$ in the interfacial region, so that the tangential velocity is at least of order $O(\Delta^2)$.
 346 Considering a zero tangential velocity yields a too-degenerate representation of the flow. We thus assume
 347 u^p small but non-zero and introduce the ansatz

$$u^p = u^p|_i, \quad v^p = v^p|_i + (y - y_i)v_y^p|_i, \quad p^p = p^p|_i - \frac{1}{Da} \left((y - y_i)v^p|_i + \frac{(y - y_i)^2}{2} v_y^p|_i \right) \quad (40)$$

348 Thus the jump conditions (13) and (16) for the tangential velocity and shear stress yield

$$u^p|_i = \frac{1 + \varepsilon_H}{2a} u_y^l|_i, \quad (41a)$$

$$\frac{1 + \varepsilon_H}{2\varepsilon_H} u^l|_i = \left[a + \frac{(1 + \varepsilon_H)(1 - 2a^2 + \varepsilon_H + 2a\xi)}{4a\varepsilon_H} \right] \delta_B u_y^l|_i. \quad (41b)$$

349 The relation (41a) is degenerate as the Darcy law is of lower order than the Darcy-Brinkman law and,
 350 therefore, cannot be enforced as a boundary condition at the fluid-porous sharp interface.

351 Substitution in the jump conditions for the pressure gradient and the normal shear stress give

$$v_{yy}^l|_i = \frac{a(1 + \varepsilon_H)}{\delta_B [a^2(\varepsilon_H - 1) - \varepsilon_H(1 + \varepsilon_H) + a(1 + \varepsilon_H)\xi]} v_y^l|_i, \quad (42)$$

$$v_y^p|_i = \frac{\varepsilon_H(1 + \varepsilon_H)}{a^2(1 - \varepsilon_H) + \varepsilon_H(1 + \varepsilon_H) - a(1 + \varepsilon_H)\xi} v_y^l|_i \quad (43)$$

352 The set of boundary conditions then reduces to the STR model (34) where

$$L = \delta_B \left[\frac{a(\varepsilon_H - 1)}{1 + \varepsilon_H} + \frac{1 + \varepsilon_H}{2a} + \xi \right], \quad F = -\frac{\xi}{\delta_B \varepsilon_H}, \quad (44a)$$

$$G = -\frac{(1 + \varepsilon_H)(a^2 - 2a\xi - \xi^2)}{2[a^2(\varepsilon_H - 1) - \varepsilon_H(1 + \varepsilon_H) + a(1 + \varepsilon_H)\xi]}, \quad (44b)$$

$$M = -\delta_B a \left[\frac{a^2[1 + \varepsilon_H(5\varepsilon_H - 2)] + 2a(\varepsilon_H^2 - 1)\xi + (1 + \varepsilon_H)^2 \xi^2}{4\varepsilon_H(a^2 + \varepsilon_H - a^2\varepsilon_H + \varepsilon_H^2 - a(1 + \varepsilon_H)\xi)} \right]. \quad (44c)$$

353 Note that, unlike (35), the expression of the coefficient G in (44) is not proportional to ξ , as a result of
 354 the dissymmetry of the pressure distributions in the fluid and porous layers introduced by the choice of the
 355 Darcy law in the interfacial region.

356 The slip length L can again be set to zero by adjusting the location of the sharp interface such that

$$\xi = \frac{1 - \varepsilon_H}{1 + \varepsilon_H} a - \frac{1 + \varepsilon_H}{2a} \quad (45)$$

357 We thus again simplify the STR model (34) into the DTR model (37) where the coefficients F , G and M are
 358 given by

$$F = -\frac{\xi}{\delta_B \varepsilon_H} = -\frac{1}{\delta_B \varepsilon_H} \left(\frac{1 - \varepsilon_H}{1 + \varepsilon_H} a - \frac{1 + \varepsilon_H}{2a} \right), \quad (46a)$$

$$G = \frac{8a^2(1 + \varepsilon_H)^2 - (1 + \varepsilon_H)^4 + 8a^4[\varepsilon_H(2 + \varepsilon_H) - 1]}{4a^2(1 + \varepsilon_H)^2(1 + 3\varepsilon_H)}, \quad (46b)$$

$$M = -\delta_B \frac{1 + \varepsilon_H[6 + 16a^4 + \varepsilon_H(4 + \varepsilon_H)]}{4a(1 + \varepsilon_H)^2(1 + 3\varepsilon_H)}. \quad (46c)$$

359 2.5 Discussion

360 So far, we have obtained three different formulations (29), (37) with (38), and (37) with (46), depending
 361 on the relative thickness $a = \Delta/\delta_B$ of the interfacial region with respect to the Brinkman penetration depth.
 362 For $a < 2$, the Darcy-Brinkman governing equations (3) are closed by the jump conditions (29) for the
 363 velocity, shear rate and pressure fields.

364 For $a > 2$, we expect the Brinkman sub-layer to be contained within the interfacial region, such that
 365 the appropriate governing equations in the porous medium are the Darcy equations (4). We obtained
 366 two similar sets of boundary conditions in that case, either by taking the limit $e^a \gg 1$ or by assuming the
 367 Darcy equations to apply within the interfacial region, which is similar to the transpiration-resistance model
 368 obtained by Lācis *et al.* [29] when written at an interface location for which the continuity of the tangential
 369 velocities replaces the Navier slip condition. However, in both cases, the resistance coefficient F is given
 370 by the same expression $F = -\xi/(\delta_B \varepsilon_H)$. Thus, the sign of F depends on the choice of the location of the
 371 sharp interface, whereas Lācis *et al.* [29] assumed it to be positive. The expression of the coefficient F
 372 can be determined rigorously, independently, without the quadrature rules employed to obtain the pressure
 373 jump condition (21) as shown in Appendix B.

374 3 Validation

375 In this section, we test the boundary conditions obtained for the TDA problem by comparing the solutions
 376 of TDA and ODA.

377 3.1 Channel flow

378 We first consider a parallel and stationary flow in a channel. The lower half of the channel is filled by
 379 a homogeneous and isotropic porous medium, and the upper half of the channel is a fluid region. The

Ratio a	Transfer model	Interface location ξ
$0 < a < \frac{1+\varepsilon_H}{2}$	Darcy-Brinkman with jump BCs (29)	$\xi = 0$
$\frac{1+\varepsilon_H}{2} < a < 2$	Darcy-Brinkman with jump BCs (29)	ξ given by (32)
$2 < a < 5$	Darcy with DTR model l(37) and (46)	ξ given by (45)
$a > 5$	Darcy with DTR model (37) and (38)	ξ given by (36)

Table 1: Summary of the different proposed representations of the mass and momentum transfer at the fluid-porous interface within the two-domain approach.

380 interfacial region extending from $y = -\Delta$ to $y = \Delta$ is modelled within the ODA by differentiable functions
381 of the form

$$\varepsilon(y) = \frac{1}{2} [1 + \varepsilon_H + (1 - \varepsilon_H) \operatorname{erf}(by)], \quad \frac{1}{\kappa(y)} = \frac{1}{2Da} [1 - \operatorname{erf}(by)], \quad (47)$$

382 where the constant b determines the extension Δ of the interfacial region. The channel height is denoted
383 by H , whereas the thickness of the porous medium is δ . The pressure gradient is adjusted so that the
384 averaged velocity is set to unity. The numerical solution to this problem has been obtained by continuation
385 methods using software AUTO07P [15]. The channel height and the extension of the porous medium are
386 set to $H = 1$ and $\delta = 0.5$, respectively, so that the fluid and porous regions have comparable sizes. The
387 homogeneous porosity was set to $\varepsilon_H = 0.41$ which is a typically reported value for packed beds [18].

388 As Δ is a crucial variable for the computation of the appropriate boundary conditions for the equivalent
389 TDA problem, we carefully adjusted the constant b by considering the numerical solutions to the GTE
390 equations (1). An example is shown in figure 2 for $Da = 10^{-4}$, $\varepsilon_H = 0.41$ and $b = 20$. The upper boundary
391 of the interfacial region may be evaluated as the location of the maximum of the shear rate u_y , i.e. $y = 0.082$,
392 which gives $\Delta \approx 1.64/b$. Hereinafter, we set $b = 2/\Delta$, thus a slightly larger evaluation of Δ , such that $\varepsilon(-\Delta)$
393 and $\kappa(-\Delta)$ depart from their constant values in the homogeneous porous region, ε_H and Da , by a relative
394 distance of only 3×10^{-3} .

395 Modifying the representation of the continuous variations of the porosity and permeability in the inter-
396 facial region has a significant but weak influence on the ODA solution. We compare in figure 3 the solutions
397 to the GTE equations (1) with the error-function representation (47) and with a hyperbolic-tangent repre-
398 sentation

$$\varepsilon(y) = \frac{1}{2} [1 + \varepsilon_H + (1 - \varepsilon_H) \tanh(b_1 y)], \quad \frac{1}{\kappa(y)} = \frac{1}{2Da} [1 - \tanh(b_1 y)] \quad \text{with} \quad b_1 = \sqrt{\pi} \ln 4 \quad (48)$$

399 where the constant b_1 has been adjusted such that the global friction exerted by the porous matrix on the
400 flow may be equivalent, i.e. $\int_0^\infty \operatorname{erf}(2y) dy = \int_0^\infty \tanh(b_1 y) dy$.

401 Figure 4 compares the solution to GTE equations (1) with and without the second Brinkman corrections
402 for $Da = 10^{-4}$ and different values of the ratio $a = \Delta/\delta_B$ of the thickness of the interfacial region to the

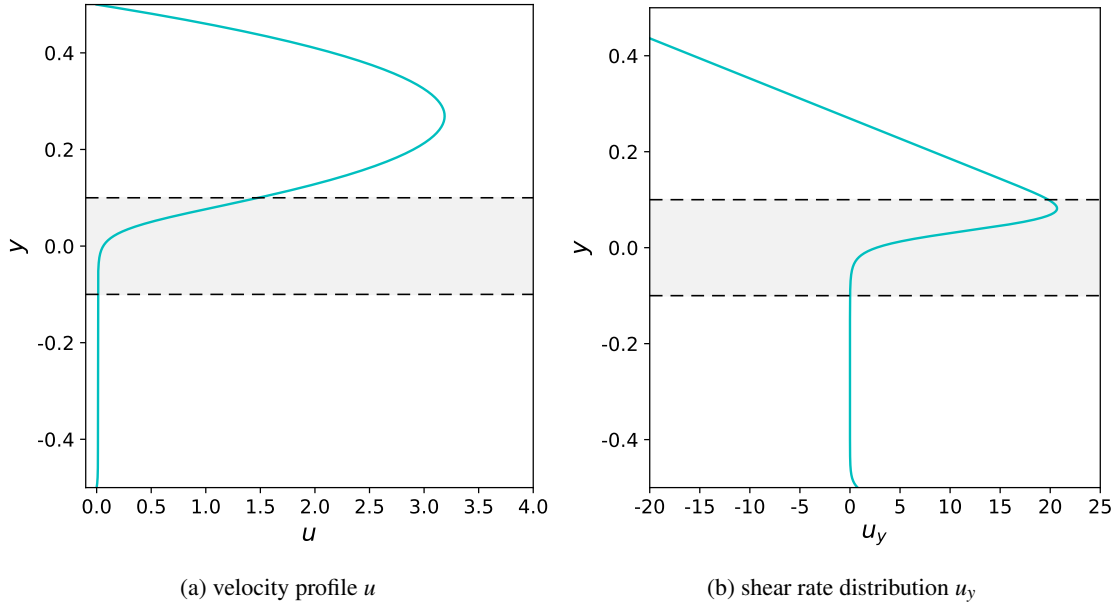


Figure 2: ODA solution to GTE (1) with error-function distributions (47) of porosity and permeability, $Da = 10^{-4}$ and $\varepsilon_H = 0.41$ and $b = 20$. The shaded band materializes the interfacial region defined by $\Delta = 2/b$.

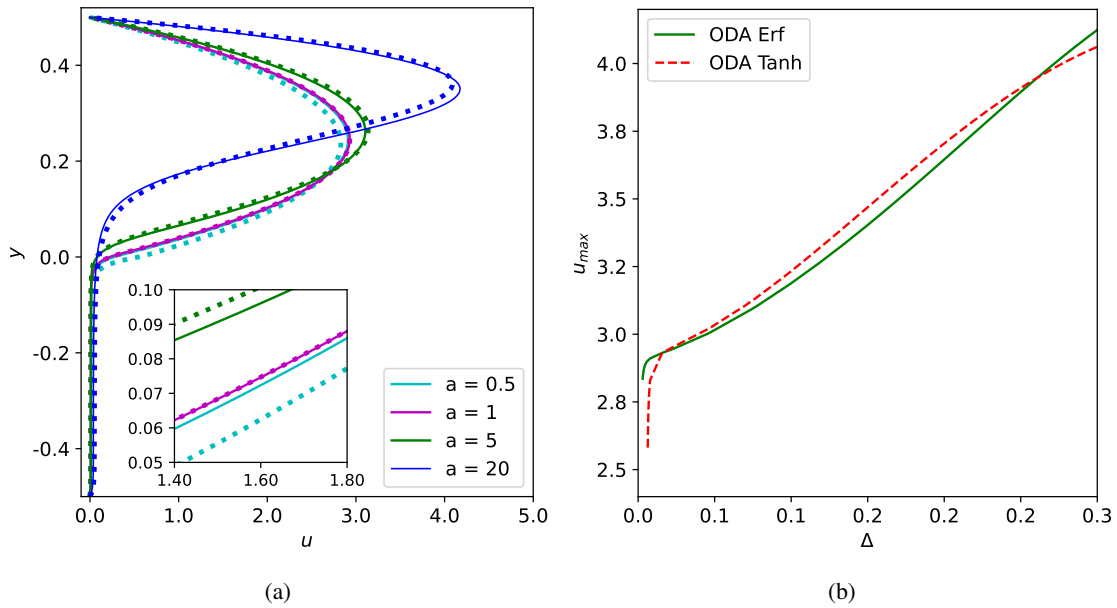


Figure 3: Comparison of ODA solutions with error-function distributions (47) of porosity and permeability (solid line), and hyperbolic-tangent distributions (48) (dashed lines) for different values of the ratio a of the interfacial region thickness Δ to the Brinkman penetration depth δ_B . Left: comparison of the velocity profiles; right: comparison of the maximum velocity u_{\max} as a function of Δ . $Da = 10^{-4}$ and $\varepsilon_H = 0.41$.

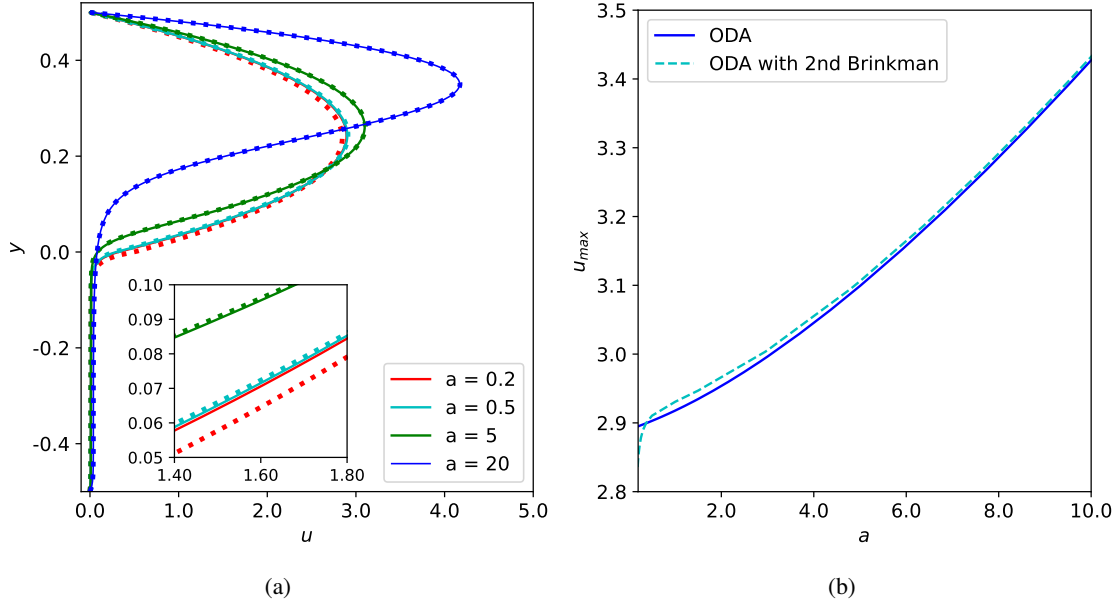


Figure 4: Comparison of ODA solutions with (dotted line) and without (solid line) second-order Brinkman corrections for different values of the ratio a of the thickness of the interfacial region to the Brinkman penetration depth. Left: comparison of the velocity profiles; right: comparison of the maximum velocity u_{\max} as functions of a . $Da = 10^{-4}$ and $\varepsilon_H = 0.41$.

403 Brinkman penetration depth. Since the first-order correction is of the order $O(\delta_B^{-2})$ and the second-order
404 corrections are of the order $O(\Delta\delta_B)$, we expect the second-order Brinkman terms to be negligible at large
405 values of a . Our computations confirm that second-order Brinkman corrections affect only weakly the ODA
406 solution whenever a is larger than 0.5. Our findings suggest that neglecting the second-order Brinkman
407 corrections is a valid simplification. Though, in agreement with Hernandez-Rodriguez *et al.* [20], we
408 observe that the difference between the ODA solutions with and without these terms decreases only slowly
409 with a .

410 We also observe that the velocity of the fluid at the inferior limit of the interfacial region, $u(y = -\Delta)$,
411 departs from the seepage velocity $-Da p_x$ by a relative value which is inferior to 10 % whenever a is larger
412 than 5 and for the tested range of porosities $\varepsilon_H \in [0.2, 0.8]$. We thus conclude that the Brinkman diffusion
413 sub-layer can be assumed to be entirely contained within the interfacial region for $a > 5$, which justifies the
414 derivation of the DTR model (37) in the thick-interface limit. Besides, for $a > 2$, the velocity in the porous
415 region remains small as $u(y = -\Delta)$ is smaller than two times the seepage velocity $-Da p_x$, which justifies
416 the use of the Darcy equations (4) and the DTR model (37) for $2 < a < 5$, even if the Brinkman sub-layer
417 is not entirely contained within the interfacial region in that case.

418 We next compute the solutions to the TDA problem using the boundary conditions we have derived in
419 section 2.2. Accuracy is assessed by comparisons to the reference ODA solutions in the fluid and porous
420 outer regions, as TDA and ODA problems differ in the interfacial region.

421 Figure 5 compares the solutions to the TDA and ODA approaches as a is varied. The thickness of the
422 interfacial region is maintained as $\Delta = 0.01$ by adjusting the Darcy number for ease of comparison. For
423 all tested values of the parameter a , an excellent agreement of the TDA and ODA solutions is observed
424 outside the interfacial region. At $a = 0.5$, the ODA solution presents large deviations of the velocity
425 profile in the porous medium from the Darcy seepage velocity, which demonstrates that the Brinkman
426 sub-layer is not contained within the interfacial region in that case. Panel a compares the solution of the
427 GTE equations (1) to the TDA solution, where the flow in the porous layer is modelled by the Darcy-
428 Brinkman law (3) and applying the jump boundary conditions (29) at the middle of the interfacial region
429 ($\xi = 0$). An excellent agreement is found. In particular, the maximum velocity of the flow is accurately
430 captured. Similar excellent agreements are observed at $a = 1.5$ (panel b) and $a = 3$ (panel c) where the

431 location of the dividing interface is adjusted with formula (32) so as to approach a near zero velocity at this
 432 interface. However, the solution to the Darcy-Brinkman equation (3) presents large deviations from the
 433 nearly constant velocity profile of the ODA solution in the vicinity of dividing interface for $a = 3$. Instead,
 434 the solution to the TDA approach modelled by the Darcy equation (4) and the DTR boundary conditions
 435 (37) accurately capture the flow in the porous medium, with the exception of the Brinkman layer at the
 436 lower wall. However, a less convincing agreement is found with the ODA solution in the fluid layer than
 437 with the TDA approach modelled by the Darcy-Brinkman equation (3) and (29). At $a = 10$, the TDA
 438 approach is modelled by the Darcy equation (4) and the DTR boundary conditions (37) with (38) or (46).
 439 The expressions (38) of the coefficients of the DTR model provide the best result with a solution in the fluid
 440 layer, which nearly coincides with the ODA solution. Indeed, the derivation of the DTR model of interfacial
 441 momentum transfer presented in section 2.3 accounts for the Brinkman sub-layer in the interfacial region,
 442 whereas the derivation of this model presented in section 2.4 assumes only a Darcy flow.

443 So far, we have compared the ODA and TDA solutions for which the boundary conditions have been
 444 derived by solving the TDA governing equations in the interfacial region in section 2.2. These boundary
 445 conditions, either (29) or the DTR model (37) are considerably more complex than the jump boundary
 446 conditions derived in section 2.1. Following Angot *et al.* [3], one may neglect the thickness of the interfacial
 447 region and directly apply on the sharp interface at $y_i = 0$ the jump conditions (13), (16), (14) and (17). Using
 448 the Darcy-Brinkman equations (3), the result is compared to the ODA solution in figure 6 for $a = 0.5$ and
 449 $a = 10$ and the same parameter set as that in figure 5. Without surprise, the agreement to the ODA solution
 450 is less convincing than when the thickness of the interfacial region is accounted for.

451 We end this section by discussing the influence of the location of the dividing interface, as defined by
 452 the parameter ξ , on the accuracy of the TDA solution with respect to the ODA solution. In our approach, the
 453 location of the dividing interface is adjusted to correspond approximately to the cancelling of the velocity
 454 in the fluid side u^l . This choice reflects the fact that the velocity in the fluid layer is much larger than in
 455 the porous layer, so the accuracy of the TDA solution corresponds principally to its capacity to represent
 456 correctly the flow in the fluid layer.

457 The location at which the velocity in the fluid layer effectively cancels can be evaluated by fitting the
 458 ODA solution by a parabola in the fluid region. Figure 7 compares the relative location of the dividing
 459 interface ξ/a obtained by this procedure to the estimates (32), (36) and (45) for two values of the porosity,
 460 $\varepsilon_H = 0.41$ and $\varepsilon_H = 0.78$. The latter value is typical of metal foam, for instance. For both cases, a
 461 reasonable agreement is found. The estimate (32) used in the range $a \in [(1 + \varepsilon_H)/2, 2]$ is particularly
 462 accurate. The estimates (32) and (45) presents the same trend as the parabolic fit to the ODA solution,
 463 whereas the estimate (36) shows a different trend. However, all three estimates converge to the same
 464 asymptote $\xi/a = (1 - \varepsilon_H)/(1 + \varepsilon_H)$ as a is increased.

465 3.2 Stagnation point

466 We extend the well-known solution of a viscous stagnation point on a solid wall [44] to the case of a
 467 porous one with suction. The porous medium extends from $y = -\delta$ to the fluid-porous boundary at $y = 0$,
 468 whereas the overlying fluid layer extends to $y = H$ with $H \gg \delta$ in order to mimic a plane irrotational flow
 469 impinging a wall. The flow is assumed to be potential far from the boundary, i.e., $u \approx x$, $v \approx -y + cst.$,
 470 $p \approx -\frac{x^2+y^2}{2} + cst.$. We introduce a suction velocity $v_s = -ADa$ at the bottom $y = -\delta$ of the porous
 471 medium. In this test case, the Darcy seepage velocity is oriented in neither normal nor tangential direction
 472 to the porous-fluid interface. Besides, $v_y \neq 0$ in the interfacial region will enable us to check the presence
 473 of pressure jumps and normal velocity. The length scale is adjusted to set the Reynolds number to unity
 474 without loss of generality.

475 Following Schlichting & Gersten [44], we introduce the ansatz:

$$476 \quad u = xf'(y), \quad v = -f(y), \quad p = -\frac{x^2}{2} - g(y), \quad (49)$$

476 which enables to reduce the resolution of the original 2D problem to a 1D one. Within the ODA approach,

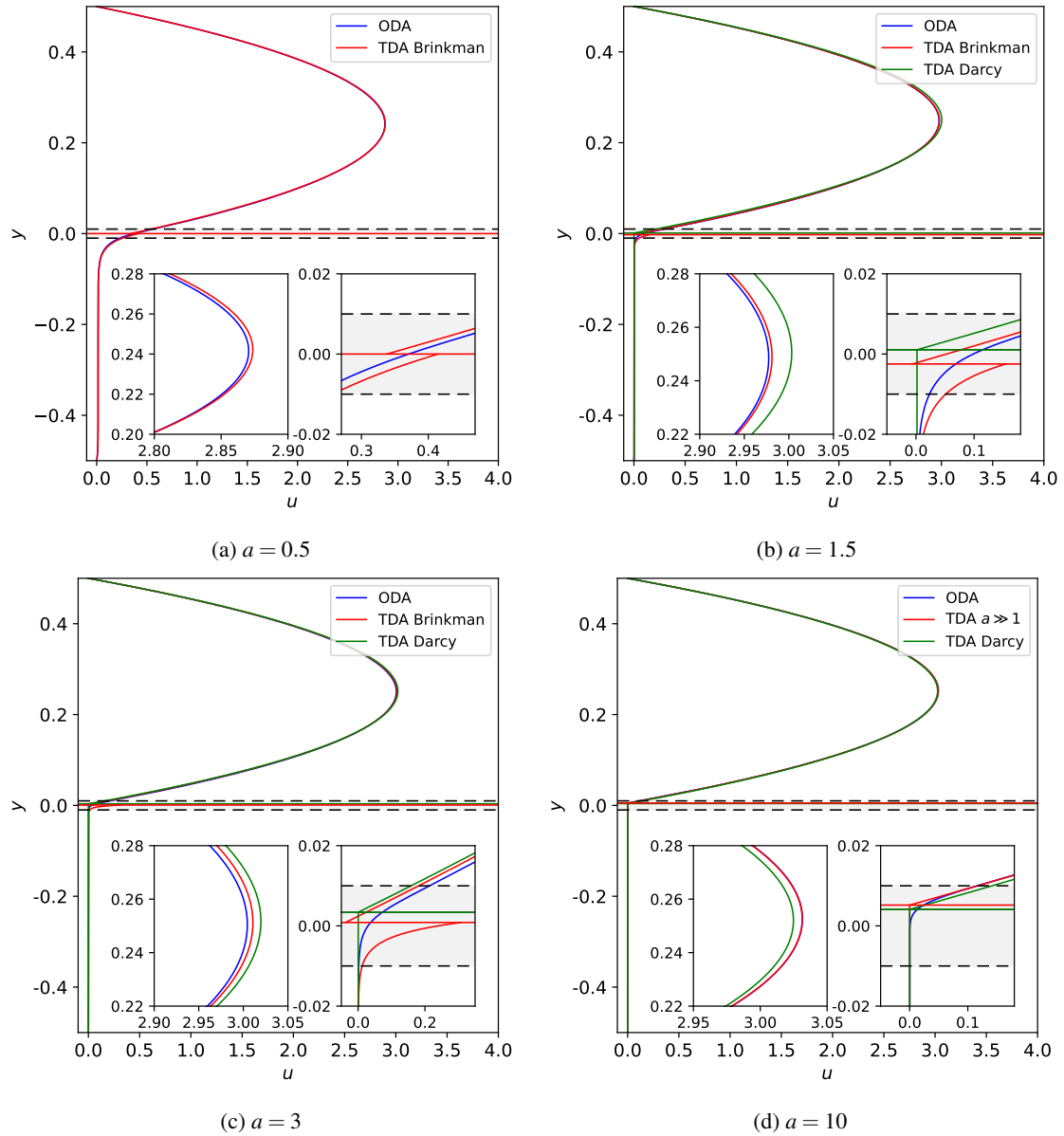


Figure 5: Comparison of ODA and TDA solutions for a constant thickness $\Delta = 0.01$ of the diffuse interface and different values of a . The Darcy number is adjusted to $Da = \epsilon_H (\Delta/a)^2$ to maintain Δ constant.

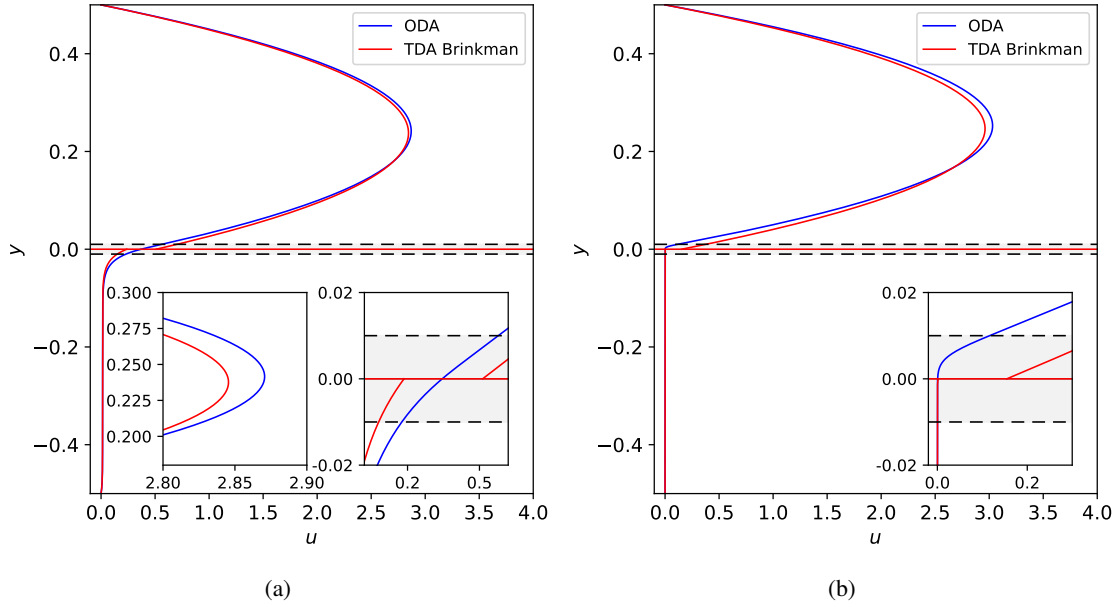


Figure 6: Comparison of ODA and TDA solutions using the jump condition (13) and (16) when applied directly at the dividing interface $y = 0$. See the caption of figure 5.

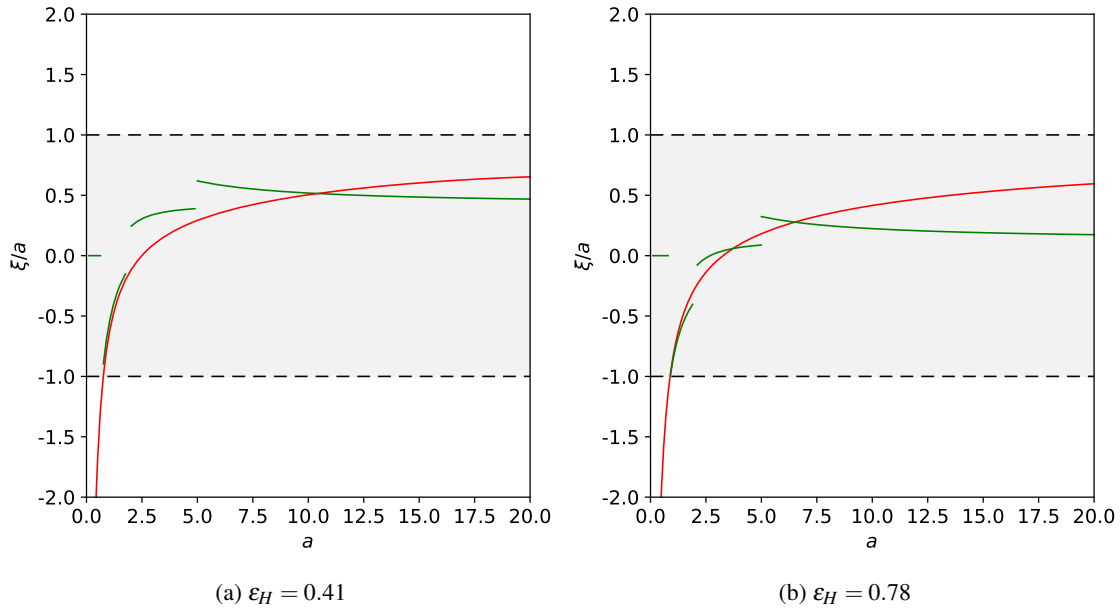


Figure 7: Estimation of the relative location ξ/a of the fluid-porous sharp interface from a parabolic fit of the ODA solution as compared to the formulae (32), (45) (36) for $Da = 10^{-4}$ and $\epsilon_H = 0.41$ (left) and $\epsilon_H = 0.78$ (right). See Table 1. The straight lines indicate the locations of the diffuse interface boundaries ($\xi = \pm a$).

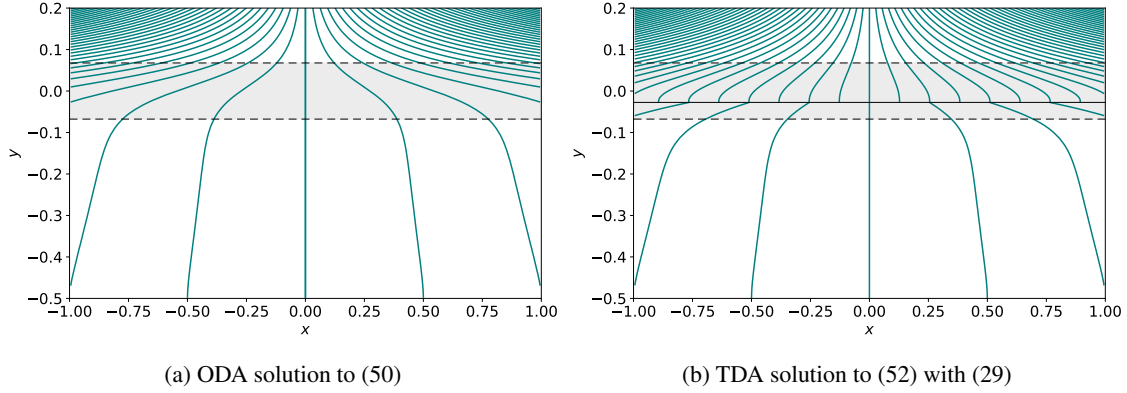


Figure 8: Streamlines in the porous region and in the vicinity of the diffuse interface (shaded regions) for the flow around a stagnation point with suction. $\delta = 0.5$, $Da = 10^{-3}$, $\varepsilon_H = 0.78$ and $a = 1.89$.

477 the system of equations to be solved thus reads

$$\frac{f'''}{\varepsilon} - \frac{f'}{\kappa} = \frac{1}{\varepsilon} \left[\frac{(f')^2 - f f''}{\varepsilon} + \frac{\varepsilon'}{\varepsilon^2} f f' \right] - 1, \quad (50a)$$

$$\frac{f''}{\varepsilon} - \frac{f}{\kappa} = \frac{1}{\varepsilon} \left[-\frac{f f'}{\varepsilon} + \frac{\varepsilon'}{\varepsilon^2} f^2 \right] + g', \quad (50b)$$

478 with the associated boundary conditions

$$f(-\delta) = A Da, \quad f'(-\delta) = g(-\delta) = 0, \quad f(H) = 1. \quad (51)$$

479 Within the TDA approach, the Darcy-Brinkman equations (3) yields

$$\frac{f^{p'''}}{\varepsilon_H} - \frac{f^{p'}}{Da} = \frac{(f^{p'})^2 - f^p f^{p''}}{\varepsilon_H^2} - 1, \quad \frac{f^{p''}}{\varepsilon_H} - \frac{f^p}{Da} = -\frac{f^p f^{p'}}{\varepsilon_H^2} + g^{p'}, \quad (52a)$$

$$f^{l''''} = (f^{l'})^2 - f^l f^{l''} - 1, \quad f^{l''} = -f^l f^{l'} + g^{l'}, \quad (52b)$$

480 which is closed by (51). Considering instead a Darcy flow within the porous medium, this system of
481 equations reduces to (52b) with $f^p = Da(A + y)$ and $g^p = -(Ay + \frac{1}{2}y^2)$.

482 We solve again systems (50) and (52) by continuation methods using AUTO07P software for the set of
483 parameters $\delta = 0.5$, $H = 10$ and $\varepsilon_H = 0.41$ or $\varepsilon_H = 0.78$. In the present test, the thickness of the interfacial
484 region is evaluated using the Carman-Kozeny relation, which relates the typical grain size d of packed beds
485 to their permeability

$$\kappa_H = \frac{\varepsilon_H^3 d^2}{180(1 - \varepsilon_H)^2}. \quad (53)$$

486 Goharzadeh *et al.* [17] estimated the thickness of the diffuse interface to correspond to the size of a grain.

487 We thus deduce from (53) an estimate for the dimensionless thickness of the interfacial region,

$$\Delta \approx 3\sqrt{5} \frac{1 - \varepsilon_H}{\varepsilon_H} \delta_B, \quad (54)$$

488 which gives $\Delta \approx 9.6\delta_B$ for $\varepsilon_H = 0.41$ and $\Delta = 1.89\delta_B$ for $\varepsilon_H = 0.78$.

489 We first consider the case of a relatively thin interfacial region, for $Da = 10^{-3}$, $\varepsilon_H = 0.78$ and $a = 1.89$.
490 Figure 8 illustrates the flow pattern and its symmetry around the stagnation point located at $x = 0$, in the
491 porous region and at the diffuse interface. The streamlines are obtained from the expression $x f(y)$ of the
492 stream function corresponding to the ODA solutions and to the TDA solution to the Darcy-Brinkman
493 equation (52) with the jump boundary conditions (29). An excellent agreement is observed in the fluid and
494 porous regions outside the diffuse interface.

495 Figure 9 further offers a direct comparison of the ODA solution to TDA solutions to the Darcy-
 496 Brinkman equation (52) with the jump boundary conditions (29), as well as to (52b) with the Darcy flow
 497 $f^p = Da(A + y)$ and $g^p = -(Ay + \frac{1}{2}y^2)$ and the DTR model (37) with (46). The Darcy-Brinkman equation
 498 with the jump conditions (29) predicts the velocity field ($u \propto f'$ and $v \propto f$) satisfactorily, even if the normal
 499 velocity in the fluid layer presents some discrepancies with the ODA solution. The velocity in the porous
 500 layer in the vicinity of the dividing interface is also somewhat overestimated. The solution to the TDA
 501 approach assuming a Darcy flow in the porous medium and using the DTR transfer model also performs
 502 satisfactorily. In particular, in both cases, the TDA approach reproduces accurately the pressure distribution
 503 within the flow represented by the function g , as well as the jump of tangential shear stress $u_y \propto f''$ across
 504 the interfacial region. Note that both (29) and (37) predict a positive jump of the pressure at the dividing
 505 interface, $p^l|_i - p^p|_i > 0$.

506 We next consider $Da = 10^{-4}$ and a porosity $\varepsilon_H = 0.41$, representative of packed beds, for which the
 507 Carman-Kozeny relation gives an estimate of the interfacial thickness corresponding to a relatively large
 508 value of $a = 9.6$. This time we compare the solution to the TDA with a Darcy flow $f^p = Da(A + y)$
 509 and $g^p = -(Ay + \frac{1}{2}y^2)$ and the DTR model (37) with (38) or (46) to the reference solution to the ODA
 510 equations (50). An excellent agreement is observed either for the coefficient expressions (38) obtained in
 511 the limit $e^a \gg 1$ or the expressions (46) obtained considering a Darcy flow in the interfacial region. As
 512 for the parallel flow considered in § 3.1, the solution to the ODA approach predicts a velocity field in
 513 the homogeneous porous region ($y < -\Delta$) which remains close to the seepage velocity $-Da\nabla p$. We thus
 514 conclude that the assumption of a Brinkman sub-layer entirely contained in the interfacial region is again
 515 justified. The DTR model, either with (38) or (46), predicts a location of the dividing interface above
 516 the centre of the interfacial region ($\xi > 0$) in close agreement with the coordinate at which the velocity
 517 predicted by the ODA solution departs from the seepage Darcy velocity. The pressure jump $p^l|_i - p^p|_i$ is
 518 then negative. A situation which is inverted with respect to the case $\varepsilon_H = 0.78$ ($\xi < 0$ and $p^l|_i - p^p|_i > 0$),
 519 and is a direct consequence of the proportionality of the resistance coefficient F with ξ .

520 4 Concluding Remarks

521 The present investigation has considered a long-standing challenge to accurately describe and model the
 522 transport phenomena in a fluid-porous medium system and the transitional region between the two domains
 523 responsible for interfacial mass and momentum transfer. Our starting point is the GTE equations (1) as a
 524 valid macroscopic description of the momentum transfer at the fluid-porous interface [20]. Following
 525 Angot *et al.* [3], we have integrated the GTE equations across the interfacial region to obtain jump boundary
 526 conditions for the speed, pressure and shear stresses. Our derivation completes the work of Angot *et al.*
 527 by taking into account the variations of the normal velocity ($v_y \neq 0$), which yields a jump condition (16)
 528 for the normal velocity instead of the continuity condition postulated by Angot *et al.* [3], Ochoa-Tapia &
 529 Whitaker [39].

530 Within the framework of TDA, the jump conditions across the interfacial regions are rewritten at the
 531 fictitious dividing interface separating the homogeneous and isotropic porous medium and the fluid layer
 532 by solving the creeping flow in the interfacial region. Two parameters are identified, namely, the Brinkman
 533 penetration depth ($\delta_B = \sqrt{Da/\varepsilon_H}$) and the ratio of the transitional thickness to the Brinkman penetration
 534 depth ($a = \Delta/\delta_B$), which facilitated the derivation of the effective homogenized boundary conditions with
 535 coefficients expressed explicitly in terms of these two parameters. For a porous medium with given poros-
 536 ity, the coefficients in the boundary conditions account for the details about the diffusive transport into the
 537 porous medium across the interface and the frictional force generated by the Darcy seepage velocity that
 538 provides resistance to the imposed shear from the fluid region. The jump conditions are imposed on a fictive
 539 interface whose location within the transitional region can be specified in terms of another parameter (ξ)
 540 that depends on the parameters δ_B and a . The exact location of the interface may be decided by requiring
 541 that the obtained TDA solutions match very closely with the corresponding ODA solutions.

542 This study proposes three different formulations depending on the parameter a . When $a < 2$, the Darcy-
 543 Brinkman equations (3) are closed by the jump conditions (29) for the velocity, shear rate and pressure
 544 distribution. For $a > 2$, two similar sets of equations are derived, either by considering the limit $e^a \gg 1$ or
 545 by assuming the Darcy equation to be valid within the interfacial region. This formulation is based on the

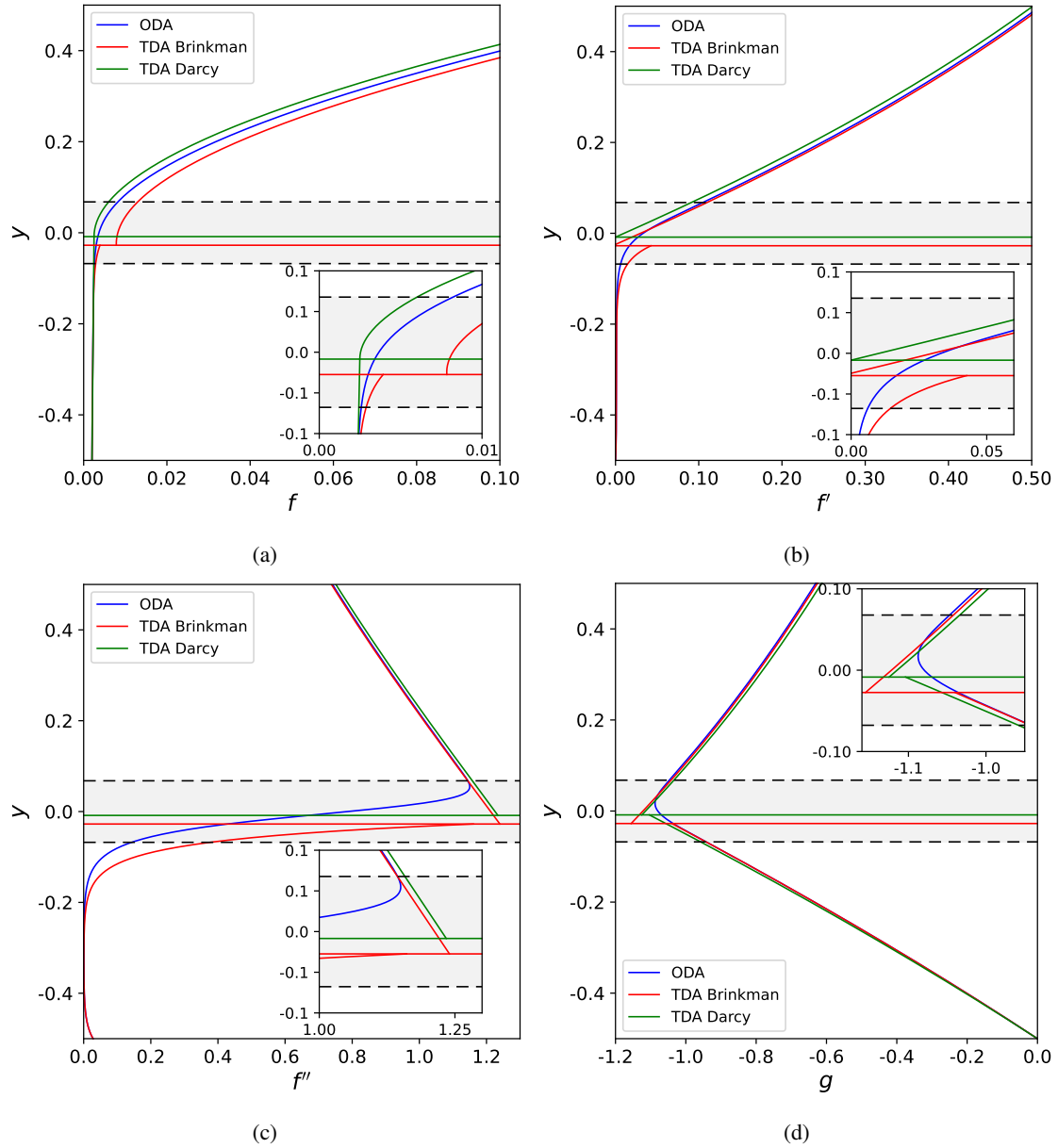


Figure 9: Comparison of ODA solution to (50), labelled ‘ODA’, with the TDA solution to (52) and (29), labelled ‘TDA Brinkman’, and with the TDA solution to (52b) and (37) with (46), labelled ‘TDA Darcy’. ($Da = 10^{-3}$, $\varepsilon_H = 0.78$, $a = 1.89$ and $A = 2$).

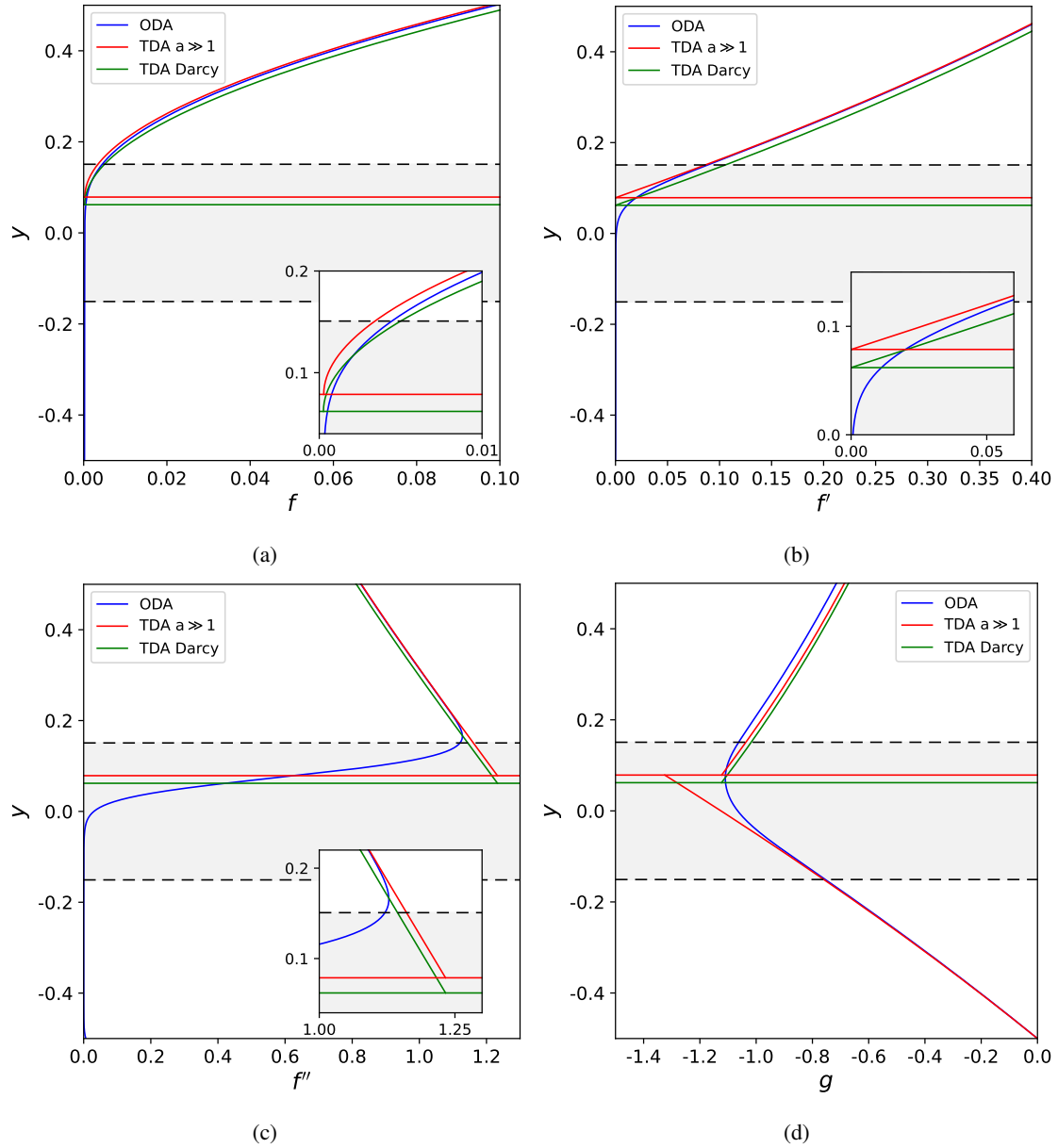


Figure 10: Comparison of ODA solution to (50), labelled ‘ODA’, with the TDA solutions to (52b) and the DTR model with (38), labelled ‘TDA $a \gg 1$ ’, and (46), labelled ‘TDA Darcy’. ($Da = 10^{-4}$, $\epsilon_H = 0.41$, $a = 9.7$ and $A = 2$).

546 consideration that the Brinkman sub-layer is contained within the interfacial region, which implies that the
 547 appropriate governing equation is the Darcy law in this case.

548 It is worth mentioning that these sets of boundary conditions resemble the slip-transpiration-resistance
 549 (STR) model (34) proposed by Lācis *et al.* [29]. The choice of the location of the sharp interface determines
 550 the sign of the resistance coefficient F , which can be determined independently of the choice of quadrature
 551 rules (see Appendix B). In this study, we choose to locate the fictitious dividing interface at a location
 552 where the fluid-side tangential velocity essentially vanishes ($u^l|_i = O(\Delta^2)$) and propose to replace the B-J
 553 slip condition by the continuity of the tangential velocity. As a result, a Dirichlet-transpiration-resistance
 554 (DTR) model (37) is proposed. The different obtained formulations and the range of the parameter a at
 555 which we propose to apply them are summarized in Table 1.

556 The derived boundary conditions have been tested by comparing the TDA solutions obtained with
 557 these boundary conditions and the corresponding ODA solutions for the following test problems: channel
 558 flow and stagnation point flow on a porous wall with suction. The satisfactory agreement of the solutions
 559 from the two approaches enhances our confidence that the proposed set of boundary conditions accurately
 560 captures the transport phenomena across the fictive sharp interface.

561 Our formulation is explicit with respect to a few geometrical parameters, which are easy to estimate
 562 in practice, and, therefore, can be easily implemented. This study is a first attempt towards a coherent
 563 mass and momentum model that complements the available models within the framework of TDA [3, 29].
 564 The proposed model presents a pathway for extending the study to multiphase flows involving fluid-porous
 565 domains and multi-scale flow problems. Further, an extension of the study to include anisotropy of the
 566 porous medium, higher dimensional flow, and inhomogeneous porous layers is feasible and may require
 567 a higher order description in terms of the interfacial thickness Δ . The investigations on these and other
 568 relevant applications are in progress.

569 Acknowledgements

570 SM thanks Vellore Institute of Technology, Vellore, India, for providing ‘VIT SEED Grant - RGEMS Fund
 571 (SG20220087)’ for carrying out this research work.

572 Declaration of Interests

573 The authors report no conflict of interest.

574 A Influence of the integration rule on the TDA boundary conditions

575 In this section, we discuss the influence of the choice of the numerical quadrature rule on the jump con-
 576 ditions across the interfacial region and the momentum transfer model for the TDA with two examples.
 577 We limit ourselves to parallel flows (i.e. $v_y = 0$) for simplicity. We show that the choice of the quadrature
 578 rule must ensure balanced jump conditions across the diffuse interfacial region in order to yield usable
 579 boundary conditions within the TDA approach.

580 A.1 Quadrature rule of a product

581 Using (9), we can write the quadrature

$$\int_a^b f(x)g(x)dx \approx \frac{h}{4}[f(a) + f(b)][g(a) + g(b)], \quad (55)$$

582 which gives

$$\int_{-\Delta}^{\Delta} \frac{u}{\kappa} dy \approx \frac{1}{2\Delta} \int_{-\Delta}^{\Delta} \frac{1}{\kappa} dy \int_{-\Delta}^{\Delta} u dy \approx \frac{1}{2D\alpha} (u|_{\Delta} + u|_{-\Delta}) \quad (56)$$

583 and

$$\int_{-\Delta}^{\Delta} \frac{u_y}{\varepsilon} dy \approx \frac{1 + \varepsilon_H}{4\varepsilon_H} (u_y|_{\Delta} + u_y|_{-\Delta}) \quad (57)$$

584 With this choice of a quadrature rule, the jump conditions connecting the fluid and porous regions within
585 the ODA approach then reads for a parallel flow ($v_y = 0$)

$$\frac{1 + \varepsilon_H}{2\varepsilon_H} (u_y|_{\Delta} - u_y|_{-\Delta}) = \frac{\Delta}{2Da} (u|_{\Delta} + u|_{-\Delta}), \quad (58a)$$

$$u|_{\Delta} - u|_{-\Delta} = \Delta (u_y|_{\Delta} + u_y|_{-\Delta}). \quad (58b)$$

586 We note that balancing the terms of the tangential stress jump (58a) implies that $u|_{\Delta} = O(Da)$ since $u|_{-\Delta} =$
587 $O(Da/\varepsilon_H)$. From (58), the following boundary conditions for the TDA problem are derived

$$(1 + \varepsilon_H + a\xi - a^2)u'_y|_i - [(1 + \varepsilon_H)C - aS]u_y^p|_i = \frac{a}{\delta_B}u'|_i - \frac{(1 + \varepsilon_H)S - aC}{\delta_B}u^p|_i, \quad (59a)$$

$$u'|_i - (C - aS)u^p|_i = -(S - aC)\delta_B u_y^p|_i. \quad (59b)$$

588 In the limit of a thick interfacial region $e^a \gg 1$, this gives

$$u'_y|_i = -\frac{(a-1)^2 + \varepsilon_H}{\delta_B(a-1)(a^2 - 1 - \varepsilon_H) - \xi[(a-1)^2 + \varepsilon_H]}u'|_i. \quad (60)$$

589 which can be rewritten as a no-slip boundary condition at an effective sharp interface located at $y_i =$
590 $\delta_B(a-1)(a^2 - 1 - \varepsilon_H)/[(a-1)^2 + \varepsilon_H] \approx a\delta_B = \Delta$, hence at the upper limit of the diffuse interfacial region.
591 This is consistent with the estimate $u|_{\Delta} = O(Da) \ll 1$, which is necessary to balance the tangential shear
592 jump (58a). Therefore, the quadrature rule (55) leads to an underestimation of the flow within the interfacial
593 region.

594 A.2 Generalization of the trapezoidal rule

595 The trapezoidal quadrature rule can be generalized with the exact formula:

$$\begin{aligned} \int_a^b f(x)dx &= \frac{h}{2}[f(a) + f(b)] + \frac{h^2}{4}[f'(a) - f'(b)] + \frac{h^3}{12}[f''(a) + f''(b)] + \frac{h^4}{48}[f'''(a) - f'''(b)] \\ &+ \dots + \frac{h^n}{2n!}[f^{(n)}(a) + (-1)^n f^{(n)}(b)] + \dots \end{aligned} \quad (61)$$

596 Denoting by $\partial_y^n u$ the n th derivative of u with respect to y , we note that $\partial_y^n (u/\kappa)|_{\Delta} \approx 0$, $\partial_y^{2n} (u/\kappa)|_{-\Delta} \approx$
597 $\delta_B^{-2n} u|_{-\Delta}$ and $\partial_y^{2n+1} (u/\kappa)|_{-\Delta} \approx \delta_B^{-2n} u_y|_{-\Delta}$. Summing the different series, we obtain after some algebra

$$\int_{-\Delta}^{\Delta} \frac{u}{\kappa} dy \approx \frac{\bar{C}\bar{S}}{\varepsilon_H \delta_B} u|_{-\Delta} + \frac{\bar{C}^2 - 1}{\varepsilon_H} u_y|_{-\Delta} \quad (62)$$

598 where $\bar{C} = \cosh a$ and $\bar{S} = \sinh a$. We have similarly

$$\int_{-\Delta}^{\Delta} \frac{u_y}{\varepsilon} dy \approx a\delta_B u_y|_{\Delta} + \frac{\delta_B \bar{C}\bar{S}}{\varepsilon_H} u_y|_{-\Delta} + \frac{\bar{C}^2 - 1}{\varepsilon_H} u|_{-\Delta} \quad (63)$$

599 We thus obtain the jump conditions

$$\frac{1 + \varepsilon_H}{2\varepsilon_H} (u_y|_{\Delta} - u_y|_{-\Delta}) = \frac{\bar{C}\bar{S}}{\varepsilon_H \delta_B} u|_{-\Delta} + \frac{\bar{C}^2 - 1}{\varepsilon_H} u_y|_{-\Delta}, \quad (64a)$$

$$\frac{1 + \varepsilon_H}{2\varepsilon_H} (u|_{\Delta} - u|_{-\Delta}) = a\delta_B u_y|_{\Delta} + \delta_B \frac{\bar{C}\bar{S}}{\varepsilon_H} u_y|_{-\Delta} + \frac{\bar{C}^2 - 1}{\varepsilon_H} u|_{-\Delta}, \quad (64b)$$

600 from which we derive the following boundary conditions at $y = \xi a$ for the TDA problem:

$$(1 + \varepsilon_H)u_y^l|_i - [(2\bar{C} - 1 + \varepsilon_H)C - 2\bar{C}\bar{S}\bar{S}] u_y^p|_i = [2\bar{C}\bar{S}C + (1 - \varepsilon - 2\bar{C}^2)\bar{S}] \frac{u^p|_i}{\delta_B}, \quad (65a)$$

$$(1 + \varepsilon_H)u^l|_i - [(2\bar{C} - 1 + \varepsilon_H)C - 2\bar{C}\bar{S}\bar{S}] u^p|_i = \delta_B [a(\varepsilon_H - 1) + \xi(1 + \varepsilon_H)] u_y^l|_i + \delta_B [2\bar{C}\bar{S}C + (1 - \varepsilon - 2\bar{C}^2)\bar{S}] u_y^p|_i \quad (65b)$$

601 In the limit of a thick diffuse interface, i.e. $e^a \gg 1$, the boundary conditions (65) give $u_y^p|_i \approx -u^p|_i/\delta_B$.
 602 Similarly, the jump conditions (64) yields $u_y|_{-\Delta} \approx -u|_{-\Delta}/\delta_B$. These estimates are obviously unphysical.
 603 They arise from the imbalance of the jump conditions (64) as \bar{C} and \bar{S} diverge to infinity in the limit $a \gg 1$.
 604 We, therefore, conclude that the quadrature rule (8) does not yield valid boundary conditions for the TDA
 605 approach.

606 B Determination of the resistance coefficient F

607 In this section, we determine the friction coefficient F in the pressure jump of the STR model (52a). We
 608 show that the expression of F is independent of the quadrature rule.

609 To this aim, we consider a parallel and steady flow normal to the fluid-porous interface, the generalized
 610 transport equations (1) yields $v = cst$ and $p_y = -v/\kappa$. As a consequence, the pressure in the liquid region
 611 is constant and equal to its value at the sharp interface location, $p = p^l|_i$, and

$$p = p^l|_i + v \int_y^\infty \frac{1}{\kappa} dy \quad (66)$$

612 Integrating the Darcy (4) or Darcy-Brinkman equation (3) similarly gives

$$p^p = p^p|_i - \frac{v}{Da} (y - y_i). \quad (67)$$

613 Requiring next that for $y \ll -\Delta$, $p = p^p$ then gives

$$p^l|_i - p^p|_i = v \left(\frac{y_i - y}{Da} + \int_\infty^y \frac{1}{\kappa} dy \right), \quad \text{for } y \ll -\Delta. \quad (68)$$

614 For an evenly distributed permeability around the middle $y = 0$ of the interfacial region we have

$$\int_\infty^y \frac{1}{\kappa} dy = \frac{y}{Da}. \quad (69)$$

615 As a consequence, we obtain

$$p^l|_i - p^p|_i = v \frac{y_i}{Da} = -F v. \quad (70)$$

616 From this we deduce the expression of the friction coefficient F such that

$$F = -\frac{y_i}{Da} = -\frac{\xi}{\delta_B \varepsilon_H} \quad (71)$$

617 which corresponds to the expressions (38) and (46).

618 References

619 [1] ALAZMI, B. & VAFAI, K. 2001 Analysis of fluid flow and heat transfer interfacial conditions between
 620 a porous medium and a fluid layer. *International Journal of Heat and Mass Transfer* **44** (9), 1735–
 621 1749.

- 622 [2] ANGOT, PHILIPPE, BOYER, FRANCK & HUBERT, FLORENCE 2009 Asymptotic and numerical mod-
623 elling of flows in fractured porous media. *ESAIM: Mathematical Modelling and Numerical Analysis*
624 **43** (2), 239–275.
- 625 [3] ANGOT, PHILIPPE, GOYEAU, BENOÎT & OCHOA-TAPIA, J. ALBERTO 2017 Asymptotic modeling
626 of transport phenomena at the interface between a fluid and a porous layer: Jump conditions. *Phys.*
627 *Rev. E* **95** (6), 063302.
- 628 [4] ANGOT, PHILIPPE, GOYEAU, BENOÎT & OCHOA-TAPIA, J. ALBERTO 2021 A nonlinear asymptotic
629 model for the inertial flow at a fluid-porous interface. *Advances in Water Resources* **149**, 103798.
- 630 [5] BASSER, HOSSEIN, RUDMAN, MURRAY & DALY, EDOARDO 2017 Sph modelling of multi-fluid
631 lock-exchange over and within porous media. *Advances in water resources* **108**, 15–28.
- 632 [6] BEAVERS, GORDON S. & JOSEPH, DANIEL D. 1967 Boundary conditions at a naturally permeable
633 wall. *Journal of Fluid Mechanics* **30** (1), 197–207.
- 634 [7] BOTTARO, ALESSANDRO 2019 Flow over natural or engineered surfaces: An adjoint homogenization
635 perspective. *Journal of Fluid Mechanics* **877**, P1.
- 636 [8] BREUGEM, WIM-PAUL & BOERSMA, BENDIKS-JAN 2005 Direct numerical simulations of turbu-
637 lent flow over a permeable wall using a direct and a continuum approach. *Physics of fluids* **17** (2).
- 638 [9] BRILLARD, ALAIN, AMRANI, JAMAL EL & JARROUDI, MUSTAPHA EL 2013 Derivation of a con-
639 tact law between a free fluid and thin porous layers via asymptotic analysis methods. *Applicable*
640 *Analysis* **92** (4), 665–689, arXiv: <https://doi.org/10.1080/00036811.2011.632768>.
- 641 [10] CARRARO, T., GOLL, C., MARCINIAK-CZOCRA, A. & MIKELIĆ, A. 2013 Pressure jump in-
642 terface law for the stokes–darcy coupling: confirmation by direct numerical simulations. *Journal of*
643 *Fluid Mechanics* **732**, 510–536.
- 644 [11] CHANDESRI, M. & JAMET, D. 2006 Boundary conditions at a planar fluid–porous interface for a
645 Poiseuille flow. *International Journal of Heat and Mass Transfer* **49** (13), 2137–2150.
- 646 [12] CHANDESRI, M. & JAMET, D. 2007 Boundary conditions at a fluid–porous interface: An a priori
647 estimation of the stress jump coefficients. *International Journal of Heat and Mass Transfer* **50** (17),
648 3422–3436.
- 649 [13] CHANDESRI, M. & JAMET, D. 2009 Jump Conditions and Surface-Excess Quantities at a
650 Fluid/Porous Interface: A Multi-scale Approach. *Transp Porous Med* **78** (3), 419–438.
- 651 [14] CIMOLIN, F. & DISCACCIATI, M. 2013 Navier–stokes/forchheimer models for filtration through
652 porous media. *Applied Numerical Mathematics* **72**, 205–224.
- 653 [15] DOEDEL, EUSEBIUS J., CHAMPNEYS, A. R., FAIRGRIEVE, THOMAS F., KUZNETSOV, YU. A.,
654 SANDSTED, BJÖRN & WANG, XIANJUN 2008 AUTO 97: Continuation And Bifurcation Software
655 For Ordinary Differential Equations (with HomCont) .
- 656 [16] GAVRILOV, KONSTANTIN, ACCARY, GILBERT, MORVAN, DOMINIQUE, LYUBIMOV, DMITRY,
657 MÉRADJI, SOFIANE & BESSONOV, OLEG 2011 Numerical Simulation of Coherent Structures over
658 Plant Canopy. *Flow Turbulence Combust* **86** (1), 89–111.
- 659 [17] GOHARZADEH, AFSHIN, KHALILI, ARZHANG & JØRGENSEN, BO BARKER 2005 Transition layer
660 thickness at a fluid-porous interface. *Physics of Fluids* **17** (5), 057102.
- 661 [18] GOHARZADEH, AFSHIN, SAIDI, ARASH, WANG, DIANCHANG, MERZKIRC, WOLFGANG &
662 KHALIL, ARZHANG 2006 An experimental investigation of the brinkman layer thickness at a fluid-
663 porous interface. In *IUTAM Symposium on One Hundred Years of Boundary Layer Research* (ed.
664 G. E. A. Meier, K. R. Sreenivasan & H.-J. Heinemann), pp. 445–454. Dordrecht: Springer Nether-
665 lands.

- 666 [19] GOYEAU, B., LHUILLIER, D., GOBIN, D. & VELARDE, M. G. 2003 Momentum transport at a
667 fluid–porous interface. *International Journal of Heat and Mass Transfer* **46** (21), 4071–4081.
- 668 [20] HERNANDEZ-RODRIGUEZ, ROEL, ANGOT, PHILIPPE, GOYEAU, BENOÎT & OCHOA-TAPIA,
669 J. ALBERTO 2022 Momentum transport in the free fluid-porous medium transition layer: One-domain
670 approach. *Chemical Engineering Science* **248**, 117111.
- 671 [21] HERNANDEZ-RODRIGUEZ, R, GOYEAU, B, ANGOT, P & OCHOA-TAPIA, JA 2020 Average veloc-
672 ity profile between a fluid layer and a porous medium: Brinkman boundary layer. *Revista Mexicana*
673 *de Ingeniería Química* **19** (Sup 1), 495–520.
- 674 [22] HILL, ANTONY A. & STRAUGHAN, BRIAN 2008 Poiseuille flow in a fluid overlying a porous
675 medium. *Journal of Fluid Mechanics* **603**, 137–149.
- 676 [23] HIRATA, S. C., GOYEAU, B. & GOBIN, D. 2009 Stability of Thermosolutal Natural Convection in
677 Superposed Fluid and Porous Layers. *Transp Porous Med* **78** (3), 525–536.
- 678 [24] HOU, J. S., HOLMES, M. H., LAI, W. M. & MOW, V. C. 1989 Boundary Conditions at the
679 Cartilage-Synovial Fluid Interface for Joint Lubrication and Theoretical Verifications. *Journal of*
680 *Biomechanical Engineering* **111** (1), 78–87.
- 681 [25] HUSSONG, JEANETTE, BREUGEM, WIM-PAUL & WESTERWEEL, JERRY 2011 A continuum model
682 for flow induced by metachronal coordination between beating cilia. *Journal of Fluid Mechanics* **684**,
683 137–162.
- 684 [26] JÄGER, WILLI & MIKELIĆ, ANDRO 2009 Modeling effective interface laws for transport phenomena
685 between an unconfined fluid and a porous medium using homogenization. *Transport in Porous Media*
686 **78**, 489–508.
- 687 [27] JIMÉNEZ BOLAÑOS, SILVIA & VERNESCU, BOGDAN 2017 Derivation of the Navier slip and slip
688 length for viscous flows over a rough boundary. *Physics of Fluids* **29** (5), 057103.
- 689 [28] LĀCIS, UĢIS & BAGHERI, SHERVIN 2017 A framework for computing effective boundary con-
690 ditions at the interface between free fluid and a porous medium. *Journal of Fluid Mechanics* **812**,
691 866–889.
- 692 [29] LĀCIS, UĢIS, SUDHAKAR, Y., PASCHE, SIMON & BAGHERI, SHERVIN 2020 Transfer of mass and
693 momentum at rough and porous surfaces. *Journal of Fluid Mechanics* **884**, A21.
- 694 [30] LĀCIS, UĢIS, TAIRA, KUNIHICO & BAGHERI, SHERVIN 2016 A stable fluid–structure–interaction
695 solver for low-density rigid bodies using the immersed boundary projection method. *Journal of Com-*
696 *putational Physics* **305**, 300–318.
- 697 [31] LEVY, THÉRÈSE & SANCHEZ-PALENCIA, ENRIQUE 1975 On boundary conditions for fluid flow in
698 porous media. *International Journal of Engineering Science* **13** (11), 923–940.
- 699 [32] LIU, QIANLONG & PROSPERETTI, ANREA 2011 Pressure-driven flow in a channel with porous
700 walls. *Journal of Fluid Mechanics* **679**, 77–100.
- 701 [33] LYUBIMOVA, T., LEPIKHIN, A., PARSHAKOVA, YA. & TIUNOV, A. 2016 The risk of river pollution
702 due to washout from contaminated floodplain water bodies during periods of high magnitude floods.
703 *Journal of Hydrology* **534**, 579–589.
- 704 [34] MIKELIC, ANDRO & JÄGER, WILLI 2000 On the interface boundary condition of beavers, joseph,
705 and saffman. *SIAM Journal on Applied Mathematics* **60** (4), 1111–1127.
- 706 [35] MOHAMMADI, A. & FLORYAN, J. M. 2013 Pressure losses in grooved channels. *Journal of Fluid*
707 *Mechanics* **725**, 23–54.

- 708 [36] MORAD, MOHAMMAD REZA & KHALILI, ARZHANG 2009 Transition layer thickness in a fluid-
709 porous medium of multi-sized spherical beads. *Exp Fluids* **46** (2), 323–330.
- 710 [37] NIELD, DONALD A, BEJAN, ADRIAN & OTHERS 2006 *Convection in porous media*, , vol. 3.
711 Springer.
- 712 [38] OCHOA-TAPIA, J. ALBERTO & WHITAKER, STEPHEN 1995 Momentum transfer at the boundary
713 between a porous medium and a homogeneous fluid—ii. comparison with experiment. *International*
714 *Journal of Heat and Mass Transfer* **38** (14), 2647–2655.
- 715 [39] OCHOA-TAPIA, J. ALBERTO & WHITAKER, STEPHEN 1995 Momentum transfer at the boundary
716 between a porous medium and a homogeneous fluid—I. Theoretical development. *International Jour-*
717 *nal of Heat and Mass Transfer* **38** (14), 2635–2646.
- 718 [40] RICHARDSON, S. 1971 A model for the boundary condition of a porous material. Part 2. *Journal of*
719 *Fluid Mechanics* **49** (2), 327–336.
- 720 [41] ROSTI, MARCO E., CORTELEZZI, LUCA & QUADRIO, MAURIZIO 2015 Direct numerical simula-
721 tion of turbulent channel flow over porous walls. *Journal of Fluid Mechanics* **784**, 396–442.
- 722 [42] SAFFMAN, P. G. 1971 On the Boundary Condition at the Surface of a Porous Medium. *Studies in*
723 *Applied Mathematics* **50** (2), 93–101.
- 724 [43] SAHRAOUI, M. & KAVIANY, M. 1992 Slip and no-slip velocity boundary conditions at interface of
725 porous, plain media. *International Journal of Heat and Mass Transfer* **35** (4), 927–943.
- 726 [44] SCHLICHTING, H. & GERSTEN, K. 2001 *Boundary-Layer Theory*. Springer Berlin Heidelberg.
- 727 [45] TAYLOR, GI 1971 A model for the boundary condition of a porous material. part 1. *Journal of Fluid*
728 *Mechanics* **49** (2), 319–326.
- 729 [46] TERZIS, A., ZARIKOS, I., WEISHAUPT, K., YANG, G., CHU, X., HELMIG, R. & WEIGAND, B.
730 2019 Microscopic velocity field measurements inside a regular porous medium adjacent to a low
731 Reynolds number channel flow. *Physics of Fluids* **31** (4), 042001.
- 732 [47] VALDÉS-PARADA, FRANCISCO J., AGUILAR-MADERA, CARLOS G., OCHOA-TAPIA, J. AL-
733 BERTO & GOYEAU, BENOÎT 2013 Velocity and stress jump conditions between a porous medium
734 and a fluid. *Advances in Water Resources* **62**, 327–339.
- 735 [48] VALDÉS-PARADA, FRANCISCO J., ALBERTO OCHOA-TAPIA, J. & ALVAREZ-RAMIREZ, JOSE
736 2007 Diffusive mass transport in the fluid–porous medium inter-region: Closure problem solution
737 for the one-domain approach. *Chemical Engineering Science* **62** (21), 6054–6068.
- 738 [49] VALDÉS-PARADA, FRANCISCO J., GOYEAU, BENOÎT & OCHOA-TAPIA, J. ALBERTO 2007 Jump
739 momentum boundary condition at a fluid–porous dividing surface: Derivation of the closure problem.
740 *Chemical Engineering Science* **62** (15), 4025–4039.
- 741 [50] VALDÉS-PARADA, F. J. & LASSEUX, D. 2021 Flow near porous media boundaries including inertia
742 and slip: A one-domain approach. *Physics of Fluids* **33** (7), 073612.
- 743 [51] VALDÉS-PARADA, FRANCISCO J., GOYEAU, BENOÎT & ALBERTO OCHOA-TAPIA, J. 2006 Dif-
744 fusive mass transfer between a microporous medium and an homogeneous fluid: Jump boundary
745 conditions. *Chemical Engineering Science* **61** (5), 1692–1704.
- 746 [52] WOOD, BRIAN D., QUINTARD, MICHEL & WHITAKER, STEPHEN 2000 Jump conditions at non-
747 uniform boundaries: the catalytic surface. *Chemical Engineering Science* **55** (22), 5231–5245.
- 748 [53] ZAMPOGNA, GIUSEPPE A. & BOTTARO, ALESSANDRO 2016 Fluid flow over and through a regular
749 bundle of rigid fibres. *Journal of Fluid Mechanics* **792**, 5–35.

- 750 [54] ZAMPOGNA, GIUSEPPE A., MAGNAUDET, JACQUES & BOTTARO, ALESSANDRO 2019 General-
751 ized slip condition over rough surfaces. *Journal of Fluid Mechanics* **858**, 407–436.
- 752 [55] ZHANG, QUAN & PROSPERETTI, ANDREA 2009 Pressure-driven flow in a two-dimensional channel
753 with porous walls. *Journal of Fluid Mechanics* **631**, 1–21.
754